eNeuro

Research Article: New Research | Disorders of the Nervous System

HIV-1 Tat and morphine differentially disrupt pyramidal cell structure and function and spatial learning in hippocampal area CA1: Continuous versus interrupted morphine exposure

https://doi.org/10.1523/ENEURO.0547-20.2021

Cite as: eNeuro 2021; 10.1523/ENEURO.0547-20.2021

Received: 16 December 2020
Revised: 27 February 2021
Accepted: 10 March 2021

HIV-1 Tat and morphine differentially disrupt pyramidal cell structure and function and spatial learning in hippocampal area CA1: Continuous versus interrupted morphine exposure

Abbreviated Title: Morphine & HIV Tat dysregulate CA1 pyramidal cells

William D. Marks[1,a], Jason J. Paris[2], Aaron J. Barbour[3,b], Jean Moon[1,c], Valerie J. Carpenter[1], Virginia D. McLane[1], Arianna R.S. Lark[1], Sara R. Nass[1], Jingli Zhang[1], Viktor Yarotskyy[1], A. Rory McQuiston[3], Pamela E. Knapp[1,3,4], Kurt F. Hauser[1,3,4]

[1] Department of Pharmacology and Toxicology, Virginia Commonwealth University, School of Medicine, PO Box 980613, Richmond, VA 23298-0613, USA

[2] Department of BioMolecular Sciences, University of Mississippi, School of Pharmacy, PO Box 1848, 315 Faser Hall, University, MS 38677-1848, USA

[3] Department of Anatomy and Neurobiology, Virginia Commonwealth University, Medical College of Virginia (MCV) Campus, PO Box 980709, Richmond, VA 23298-0709, USA

[4] Institute for Drug and Alcohol Studies, Virginia Commonwealth University, Medical College of Virginia (MCV) Campus, Richmond, VA 23298, USA

4. Author contributions: WDM, ARM, and KFH Designed research, WDM, JJP, AJB, JM, VJC, VDM, ARSL, SRN, JZ, and VY Performed research, WDM, JJP, AJB, JM, VJC, VDM, ARSL, SRN, VY, ARM, and KFH Analyzed data, WDM, JJP, VDM, VY, ARM, PEK, and KFH Wrote the paper.

5. Correspondence should be addressed to: Kurt F. Hauser, Ph.D.; Department of Pharmacology and Toxicology, Virginia Commonwealth University; Molecular Medicine Research Building, Room 4040; 1220 East Broad Street, P.O. Box 980613; Richmond, Virginia 23298-0613; Phone: (804) 628-7579; Fax: (804) 828-0676; Email: kurt.hauser@vcuhealth.org

[a]Author's present address: Department of Psychiatry, University of Texas Southwestern Medical Center, Dallas, TX 75235

[b]Author's present address: Department of Neurology, University of Pennsylvania, Philadelphia, PA 19104

[c]Author's present address: Department of Pharmacology, Case Western Reserve University School of Medicine, Cleveland, OH 44106

6. Figures: 7 **7. Tables:** 2 **8. Number of Multimedia:** 0

9. Abstract: 223 words **10. Significance Statement:** 116 words **11. Introduction:** 779 words

12. Discussion: 1779 words

13. Acknowledgements: The authors gratefully acknowledge support from the National Institute on Drug Abuse.

14. Conflict of Interest Statement: Authors report no conflict of interest

15. Funding sources: This work was supported by funds from the National Institutes of Health, R01 DA018633 (KFH), R00 DA039791 (JJP), R01 MH107507 (ARM), R01 DA034231 (PEK & KFH), K02 DA027374 (KFH), F31 DA047195 (AJB), F32 DA047193 (VDM), and T32 DA007027.

Abstract

About half the people infected with HIV have neurocognitive deficits that often include memory impairment and hippocampal deficits, which can be exacerbated by opioid abuse. To explore the effects of opioids and HIV on hippocampal CA1 pyramidal neuron structure and function, we induced HIV-1 Tat expression in transgenic mice for 14 d and co-administered time-release morphine or vehicle subcutaneous implants during the final 5 d (days 9-14) to establish steady-state morphine levels. Morphine was withheld from some *ex vivo* slices during recordings to begin to assess the initial pharmacokinetic consequences of opioid withdrawal. Tat expression reduced hippocampal CA1 pyramidal neuronal excitability at lower stimulating currents. Pyramidal cell firing rates were unaffected by continuous morphine exposure. Behaviorally, exposure to Tat or high dosages of morphine impaired spatial memory. Exposure to Tat and steady-state levels of morphine appeared to have largely independent effects on pyramidal neuron structure and function, a response that is distinct from other vulnerable brain regions such as the striatum. By contrast, acutely withholding morphine (from morphine-tolerant *ex vivo* slices) revealed unique and selective neuroadaptive shifts in CA1 pyramidal neuronal excitability and dendritic plasticity, including some interactions with Tat. Collectively, the results show that opioid-HIV interactions in hippocampal area CA1 are more nuanced than previously assumed, and appear to vary depending on the outcome assessed and on the pharmacokinetics of morphine exposure.

Significance Statement: HIV-1 transgenic mice were co-exposed to Tat and morphine to explore opioid-HIV interactions in hippocampal area CA1. Spatial memory was impaired by both Tat and morphine. Tat expression reduced the firing rate of hippocampal CA1 pyramidal neurons at lower stimulating currents irrespective of morphine exposure. Exposure to Tat and steady-state levels of morphine acted in a largely independent manner to alter pyramidal

neuron structure, function, and associated behavior. This makes CA1 distinct from other regions such as the striatum. Alternatively, withholding morphine (from morphine-tolerant *ex vivo* slices) revealed unique, but subtle, neuroadaptive shifts in pyramidal neuronal excitability and dendritic plasticity, suggesting that opioid-HIV interactions in the hippocampus are markedly influenced by the pharmacokinetics of opioid exposure.

Introduction

Human immunodeficiency virus-1 (HIV-1) infection results in neurocognitive impairments collectively termed HIV-associated neurocognitive disorders (HAND). Diminished spatial and verbal memory, frequently associated with hippocampal dysfunction, are hallmarks of HAND (Maki et al., 2009; Meyer et al., 2013; Keutmann et al., 2017). These and other deleterious HIV related outcomes are aggravated by opiate abuse (Lucas et al., 2002; Denis et al., 2019). The opioid epidemic, which has partially driven the HIV pandemic (Nath et al., 2002; Campbell et al., 2017; Fitting et al., 2020), may impede current goals to eradicate HIV within 10 years (Fauci et al., 2019; Lerner and Fauci, 2019). Despite the prevalence of people infected with HIV (PWH) who are chronically exposed to opiates, the mechanisms underlying the neuropathological effects of HIV and morphine are incompletely understood.

The HIV-1 regulatory protein, transactivator of transcription (Tat), is intrinsically neurotoxic and has been shown to impair spatial memory in mice (Carey et al., 2012; Kesby et al., 2016; Marks et al., 2016). Morphine exerts similar antimnemonic effects (Zhu et al., 2011; Kitanaka et al., 2015). Previous work has identified HIV-1 Tat-induced reductions of long-term potentiation (LTP) in CA1 pyramidal neurons, which coincided with spatial memory deficits in Tat transgenic mice (Li et al., 2004; Fitting et al., 2013). This prior work showed only modest changes in synaptic spine density and no differences in excitatory synaptic protein content.

However, Tat markedly reduced expression of synaptotagmin 2 (Syt2), while triggering presumably compensatory increases in gephyrin postsynaptically, suggesting losses in inhibitory GABAergic transmission within CA1 (Fitting et al., 2013). This selective vulnerability of interneurons within the CA1 may lower the threshold of excitation, leading to an increased likelihood of excitotoxicity. Dysregulation of excitatory/inhibitory tone may involve specific interneuronal subtypes and microcircuits (Fitting et al., 2013; Marks et al., 2016).

Opioid use disorder (OUD) can promote neurodegeneration within the hippocampus and other brain regions. Chronic abuse was found to accelerate Alzheimer's disease-like pathology in multiple brain areas including the hippocampus of HIV-negative individuals in a cohort of preferential opiate misusers in Edinburgh, Scotland (Ramage et al., 2005; Anthony et al., 2010; Kovacs et al., 2015). This includes increases in hyperphosphorylated tau, GSK3β, and CDK5 levels, as well as microgliosis (Anthony et al., 2010). Within the hippocampus, opiate abuse alters CA1 ensemble activity (Liu et al., 2010) and impairs CA3-CA1 LTP (Borjkhani et al., 2018). Opiate abuse is linked to white matter damage (Li et al., 2016), and increased systemic inflammation (Piepenbrink et al., 2016). Even among PWH treated with combination antiretroviral therapy (cART), OUD (which often includes cocaine co-exposure) worsens HAND symptomatology—including deficits in verbal and working memory (Byrd et al., 2011; Byrd et al., 2012; Meyer et al., 2013) and decision making (Boraud et al., 2013). Within the microcircuitry of hippocampal subregions, opiates and Tat may exert unique interactions. Morphine generally decreases interneuron excitability (Liao et al., 2005; McQuiston, 2008; Xu et al., 2013; Fitting et al., 2015; Fitting et al., 2016); however, morphine's capacity to inhibit GABAergic interneuronal inputs onto pyramidal cells may also exacerbate Tat-induced excitotoxicity. These outcomes are dependent on neuronal type and opioid receptor distribution (Drake and Milner, 2002; Liao et al., 2005; McQuiston, 2007, 2008; Xu et al., 2013).

OUD can exacerbate HIV-induced neuropathology across multiple brain regions (Fitting et al 2010a; Fitting et al 2014; Hauser et al, 2012; Hahn et al., 2016; Fitting et al, 2020),

112 although due to the regional differences in the development of HIV-induced pathology and μ-
113 opioid receptor expression, each brain region is anticipated to display unique pathological
114 interactions and rates of decline (Fitting et al, 2010b). Given the Tat-mediated deficits
115 previously observed in the GABAergic network of the mouse hippocampus, we hypothesized
116 that the expression of Tat would disrupt the functional output of CA1, and that morphine would
117 exacerbate these effects. We further expected that the reduction of Syt2 in the stratum
118 radiatum (SR) layer of CA1 would result in a loss of synaptic contacts on pyramidal cells. To
119 test these hypotheses, control and Tat transgenic mice were implanted with subcutaneous
120 vehicle or morphine (25 mg) time-release implants. Mice were assessed for effects on spatial
121 memory and motor behavior. Opioid injection drug use is accompanied by fluctuating drug
122 levels (Kreek, 1987, 2001; Kreek et al., 2002) resulting in 3-4 bouts of "relative withdrawal" per
123 day between injections (Reisine and Pasternak, 1996). To begin to assess the initial
124 pharmacokinetic consequences of opioid withdrawal, morphine was withheld from some *ex vivo*
125 slices during recordings. CA1 pyramidal cell function was studied via whole-cell patch-clamp
126 electrophysiology in *ex vivo* slices in the presence or absence of morphine. Patched pyramidal
127 cells were then visualized via biocytin backfill and 3-D reconstruction, and morphology was
128 assessed.
129

130 **Materials and Methods**

131 The use of mice in these studies was preapproved by the Institutional Animal Care and Use
132 Committee at Virginia Commonwealth University. Experiments were conducted in accordance
133 with ethical guidelines defined by the National Institutes of Health (NIH Publication No. 85-23).

134 *Subjects and housing.*

This study utilized male mice between 8 and 12 weeks of age with or without the presence the HIV-1 *tat* transgene (HIV-1 Tat_{1-86}) under the control of a doxycycline-activated Tet-on expression system driven by a glial fibrillary acidic protein (GFAP) promoter (Bruce-Keller et al., 2008). Doxycycline (Dox) was administered in a specially formulated diet (Dox Diet #2018, 6 g/kg, Harlan Laboratories, Madison, WI) to the mice for 14 d, after which tissues were harvested for biochemical or electrophysiological experiments. All mice were housed 4-5/cage and maintained in a temperature- and humidity-controlled room on a 12:12 h light/dark cycle (lights off at 18:00 h) with food and water available *ad libitum*. On day 5 of Dox administration, vehicle or morphine pellets (25 mg morphine sulfate, NIDA Drug Supply System, Bethesda, MD) were implanted subcutaneously.

Surgical procedure.

Subcutaneous vehicle- or morphine-containing pellets were implanted in Tat− ($n_{vehicle}$ = 17, $n_{morphine}$ = 15) and Tat+ ($n_{vehicle}$ = 18, $n_{morphine}$ = 15) mice under isoflurane anesthesia (2.5-4%) as described previously (Fitting et al., 2016). Following surgery, mice were monitored for 96 h to ensure weight gain, muscle tone, proper neurological response, and general health (Crawley and Paylor, 1997). All mice in the present study recovered.

Ex vivo *slice preparation for electrophysiological experiments.*

Following 14 days of Dox exposure, adult male mice were over-anesthetized with isoflurane anesthesia (5%), euthanized, and transcardially perfused with sucrose cutting media (in mM; 3 KCl, 4.12 $MgSO_4$, 1.2 NaH_2PO_4, 206 sucrose, 25 $NaHCO_3$, 25 glucose) chilled to 1-3 °C and bubbled with a 5% CO_2 balanced oxygen mix. Brains were dissected, bisected midsagittally, and 350-µm-thick, horizontal sections were cut from the ventral surface using a Leica VT1200 S vibratome (Leica Biosystems, Buffalo Grove, IL). Slices were cut in oxygenated sucrose cutting media held at 1-3 °C by an external cooling apparatus (Huber, Offenburg, Germany),

159 then transferred onto a nylon mesh submerged in oxygenated extracellular recording solution
160 (in mM; 3 KCl, 1.2 $CaCl_2$, 1.2 $MgSO_4$, 1.2 NaH_2PO_4, 125 NaCl, 25 $NaHCO_3$, 25 glucose) and
161 maintained at 36.5 °C for 30 min. In slices in which morphine is maintained (not withheld), the
162 cutting solution and extracellular solution were supplemented with 500 nM morphine sulfate.
163 The beaker was then returned to room temperature and the slices allowed to rest for 30 min
164 prior to recording. In parallel experiments, morphine sulfate was withheld from the cutting and
165 extracellular solutions to model acute (2-4 h) withdrawal in morphine-pelleted mice.

166 *Electrophysiological recording.*

167 Slices were continuously perfused with extracellular recording solution warmed to 30-34 °C with
168 an external heating apparatus (Warner Instruments, TC-344B, Hamden, CT, USA). The CA1
169 subfield of the hippocampus was visualized using a 4× magnification objective on a Zeiss Axio
170 Examiner A1 microscope (Zeiss, Oberkochen, Germany). Magnification was switched to a 63×
171 fluid-immersion objective to identify putative pyramidal neurons in the CA1 pyramidal layer.
172 Pipettes for whole-cell patch-clamp physiology were pulled (Narishige PC-10 pipette puller;
173 Narishige, Tokyo, Japan) from borosilicate glass pipettes (WPI #1B1505-4, World Precision
174 Instruments, Sarasota, FL, USA) to a resistance of 2-6 MΩ. Pipettes were filled with an
175 intracellular solution containing (in mM) 135 $KMeSO_4$, 10 HEPES, 2 MgATP, 0.1 NaGTP, 8
176 NaCl, 0.1 $BAPTAK_4$, biocytin 0.2% (pH 7.25). Membrane potentials were recorded using a
177 MultiClamp 700B amplifier (Molecular Devices, Sunnyvale, CA, USA), processed using a
178 Digidata 1550A digitizer, and analyzed using Clampex 10.4 software (Molecular Devices,
179 Sunnyvale, CA, USA) on a Microsoft Windows-based computer. Membrane potentials were
180 observed in response to stepwise, 25 pA current increases from −100 pA to 400 pA.

181 *Histological processing of biocytin-filled pyramidal cells.*

182 After completion of electrophysiological recordings, slices containing biocytin-filled cells were
183 moved into a 24-well plate and fixed with 4% paraformaldehyde in 1× phosphate buffered

saline (PBS) for 4-7 days at 4 °C. Following fixation, slices were rinsed in PBS 6 times for 10 min each on a rocking platform at 4 °C. Slices were permeabilized for 30 min in a solution of 50% ethanol in 1× PBS, containing 0.02% Triton X100, then transferred into a similar solution containing 70% ethanol for 30 min, and returned to 50% ethanol for 30 min. Slices were rinsed as described earlier, and then blocked in PBS containing 2% normal chicken serum, 0.02% bovine serum albumin, and 0.02% Triton X100 for 30 min. Primary antibodies against gephyrin (goat polyclonal, 1:1000, Sc-6411, Santa Cruz, Dallas, TX, USA) were applied, and slices were incubated for 48 h on a rocking platform at 4 °C. The slices were rinsed as before and incubated in secondary antibodies (donkey anti-goat IgG-Alexa Fluor® 488 1:500, Invitrogen A1055; goat anti-rabbit IgG-Alexa Fluor® 647 1:500, Invitrogen A-21244), as well as an Alexa Fluor® 594 Conjugated streptavidin probe to label biotin (1:100, Invitrogen, S-32356) for 48 h, and then rinsed in PBS. Slices were incubated in Hoechst 33342 at room temperature (0.5 µg/ml in PBS; Invitrogen, H3570) for 10 min, rinsed in PBS, and mounted on slides using ProLong Gold Antifade reagent (Invitrogen, P36930).

Imaging, 3-D reconstruction, and analysis of biocytin-filled pyramidal cell dendrites.

Z-stack imaging of neurons was performed using a Zeiss LSM 700 at 20× (plan-apochromat 0.8 NA, M27) and 63× (plan-apochromat 1.40 NA oil immersion DIC, M27) magnification (Zeiss, Oberkochen, Germany). Hoechst 33342 was visualized using a 405 nm laser with a SP 490 nm filter, Alexa Fluor 488 using a 488 nm laser and a BP 490-555 nm filter, and Alexa Fluor 594 using a 555 nm laser with the variable secondary dichroic (VSD) beamsplitter set at 585 nm. Z-Stack data was reconstructed into a 3-D image using Imaris Bitplane 7.6.4 (Zurich, Switzerland). Primary dendrites were defined as dendrites that protrude from the cell body, with dendritic order increased by every branching point. Dendritic spine analysis was performed by a blinded observer using Imaris Bitplane 7.6.4 and regions selected for analysis were 20-30 µm in length and were selected at a 5-10 µm distance from the previous branch

point and at least 5 μm from the next branch point. Dendritic spine densities are reported as the average number of spines per 10 μm length of dendrite/cell. Spine morphology was analyzed using uncompressed Z-stacks. Spines were counted along 20-30 μm long dendrite segments parallel to the plane of view. The dendritic spine density determinations of the vehicle versus the morphine-replete groups, and the vehicle versus the morphine-withheld groups, were performed separately by separate individuals. Accordingly, the spine densities in the vehicle (control) groups in the morphine-replete and morphine-withheld groups differ from one another.

Quantification of spine subtypes using ImageJ

In brief, mushroom, stubby, and thin/filopodial subtypes were identified in fluorescent images by a blinded observer, as described previously (Schier et al., 2017). Dendritic spines along a ~30 μm segment of dendrite parallel to the plane of the z-slice were counted. Dendritic segments were analyzed within the SO, SR, and SL-M anatomical strata of backfilled CA1 pyramidal neurons. Data are expressed as number of spines/10 μm-length of dendrite from individual cells.

Quantification of inhibitory puncta

Analysis of inhibitory puncta associated with specific neurite segments was performed using the co-localization module of Imaris Bitplane [version 9.0]. Briefly, background signal was filtered out of the 488 nm channel (gephyrin), and the signal from the 594 nm channel (streptavidin-tagged pyramidal cells) was used as a mask to create a co-localization channel for gephyrin puncta occurring within spaces occupied by filled pyramidal cells. The number of puncta was quantified along approximately 10 μm of the identified neurite segment. Data are expressed as the number of gephyrin-labeled puncta per micrometer. Analysis of inhibitory contacts took place on the aspinous portions of the apical and basilar dendrites immediately adjacent to the cell body, as well as the spiny portions at the distal ends of dendrites

terminating in SL-M, as these dendritic compartments have the greatest percentage of extant inhibitory contacts on a " representative" CA1 pyramidal cell (Megıas et al., 2001).

Stereology.

The volume fraction (V_V) of hippocampal areas CA1, CA2, CA3, and the dentate gyrus were assessed stereologically. Tat− and Tat+ (*n* = 5-6) mice were administered vehicle or 25 mg morphine (*not shown*) time-release pelleted implants, perfused with 4% PFA and frozen at −80 °C. Frozen hippocampal sections were sectioned 40-μM thick in the coronal plane and stained with Hoechst 33342 (1:20,000 in PBS, 8 min at room temperature). Left hemispheres were imaged at 10× magnification and montaged using a Zeiss Axio-Observer Z1 microscope with a motorized stage encoder and computerized tile-reconstruction (Zeiss, Zen Black 2.3). V_V was estimated using point count analysis and a standardized grid overlay (per Cavalieri's principle; West et al., 1991; Calhoun et al., 1998; Mouton, 2002, 2014).

Barnes maze task.

All behavioral testing was conducted in the presence of 70 dB white noise with mice habituated to the testing room for 1 h prior to assessments. Behavioral data were recorded and digitally encoded using an ANY-maze animal tracking system (Stoelting Co., Wood Dale, IL).

Mice were assessed for spatial learning and motor function via the Barnes maze (Barnes, 1979) as modified from previously reported methods (Marks et al., 2016). After a day of surgical recovery, mice were prehabituated to the maze (day 1) followed by 4 days of testing (2 trials per day over days 2-5), and a 1-day reversal probe trial (2 trials on day 6). Briefly, on day 1, mice were prehabituated to a random escape hole for 2 min, then were placed in the brightly lit center of the Barnes maze [91 cm diameter, 90 cm height, with 20 holes (each 5 cm diameter; Stoelting Co., Wood Dale, IL) and guided to the escape hole where they remained for 2 min. Lastly, mice were placed under a glass cylinder next to the escape hole and allowed to volitionally enter (3 min max. latency), or were guided in, and remained for 2 min. On testing

days, mice were placed in the brightly lit center of the Barnes maze and allowed up to 3 min to find an open escape hole (escape-hole quadrant counter-balanced across testing groups). Mice that did not enter the hole were gently guided to the hole and allowed to remain for 2 min. On the final day of testing, a reversal probe trial was conducted such that the correct goal box was rotated 180° from its original position. The mean response of both trials was analyzed on each day for all mice. Shorter latencies to find the escape hole, a greater proportion of time spent in the correct quadrant of the maze, and fewer errors were considered indices of greater learning (Camara et al., 2013). Distances and velocities traveled were used as motor indices (Marks et al., 2016).

Vision testing.

All mice were tested for visual function following conclusion of the Barnes maze test (Wersinger et al., 2002; Marks et al., 2016). Briefly, mice were suspended approximately 30.5 cm above a vertical ring-stand and were lowered with the ring-stand approximately 30.5 cm from the left or right visual field (close enough to allow visual, but not whisker, contact with the ring-stand). The left and right visual fields were assessed for each mouse, with the starting side counterbalanced across groups. Visual responding was considered positive when mice reached with the forepaws for the rod when presented to both the left and right side. A response to only one visual field is considered a negative response. One male animal (Tat+/morphine) failed vision testing and was excluded from analyses.

Statistical analyses.

Electrophysiological measures were assessed via repeated measures ANOVA (firing frequency) or two-way ANOVA (intrinsic membrane properties) with current step as the within-subjects factor (0-400 pA), and tissue genotype (Tat− or Tat+) and drug treatment combination (vehicle exposed tissues, morphine-exposed tissue in morphine-free solution, or morphine-exposed tissue in morphine-replete solution) as the between-subjects factors. *A priori* planned

comparisons were conducted on all electrophysiological data with morphine-exposed Tat− and Tat+ tissues (maintained in either morphine-replete or morphine-withheld solution) compared to their respective vehicle controls, with Bonferroni corrections for multiple comparisons applied. The density of dendritic spines was assessed separately by spine type via two-way ANOVA with tissue genotype (Tat− or Tat+) and drug treatment combination (vehicle-exposed tissues, morphine-exposed tissue in morphine-free solution, or morphine-exposed tissue in morphine-replete solution) as the between-subjects factors. Fisher's protected least significant difference (PLSD) *post hoc* tests were used to assess group differences following main effects. Interactions were delineated via simple main effects and main effect contrasts with alpha corrections for multiple comparisons. Behavioral data were assessed via repeated-measures ANOVA with Barnes maze testing trial (testing days 1-4 and reversal probe) as the within-subjects factor, and both mouse genotype (Tat− or Tat+) and drug treatment (morphine or vehicle) as the between subjects factors. Fisher's protected least significant difference (PLSD) *post hoc* tests were used to assess group differences following main effects. Interactions were delineated via simple main effects and main effect contrasts with alpha corrections for multiple comparisons. Effect size measures (η^2, Cohen's *d*) are presented following omnibus inferential statistics and main effect contrasts, respectively. All analyses were considered significant when $p < 0.05$.

Results

Morphine and Tat influence the electrophysiological properties of CA1 pyramidal cells

We used whole-cell patch-clamp physiology to examine the firing frequency and other electrophysiological properties of CA1 pyramidal cells, as they represent the focal point of inhibitory and excitatory processing in the region before projecting out toward the entorhinal cortex. To assess the effects of Tat and morphine on physiological function of CA1 pyramidal

cells as the functional output of CA1, a planned comparison testing approach was applied to assess the statistical differences between six sets of conditions: Tat− and Tat+ vehicle-treated mice (n = 13 cells from 3 mice, and 11-12 cells from 3 mice, respectively), Tat− and Tat+ morphine treated mice in which the *ex vivo* slices were continuously maintained in 500 nM morphine-containing physiological solutions during recordings and referred to as 'morphine-replete' (n = 19 cells from 4 mice, and 13 cells from 4 mice, respectively), and Tat− and Tat+ morphine-treated mice in which morphine was withheld from the *ex vivo* slices that were maintained in physiological solutions lacking morphine during recordings and referred to as 'morphine withheld' (n = 29 cells from 8 mice, and 22 cells from 7 mice, respectively). Tat− and Tat+ vehicle-treated mice were independently compared to 'morphine-replete' groups or to 'morphine-withheld' groups (Fig 2), but 'morphine-replete' and 'morphine-withheld' groups were not directly compared to one another.

When comparing Tat− and Tat+ vehicle-treated mice to Tat− and Tat+ morphine-replete mice, several effects were observed (Fig. 1*A,C,E-G*). Repeated-measures assessment of firing frequency showed a significant interaction between current step and Tat genotype [$F_{(15,780)}$ = 3.04, $p < 0.05$; $\eta^2 = 0.007$] (Fig. 1*A,C*). *Post hoc* contrasts revealed that between the 50 pA and 150 pA current steps, pyramidal cells from Tat+ mice fired at a lower frequency than those from Tat− mice (p = 0.002 - 0.046; Cohen's d = 0.5 - 0.8; Fig. 1*C-D*). Intrinsic membrane properties were assessed by two-way ANOVA. An interaction between Tat and morphine exposure was observed in the resting membrane potential of the CA1 pyramidal cells [$F_{(1,53)}$ = 7.34, $p < 0.05$; $\eta^2 = 0.12$]. Pairwise comparisons using the Bonferroni correction for multiple comparisons (significance threshold set at $p < 0.008$) revealed that only vehicle-treated Tat− and Tat+ mice differed (Fig. 1*E*), with Tat+ vehicle treated mice having significantly more depolarized resting membrane potentials (p = 0.006; Cohen's d = 1.2). In addition, a main effect of morphine was observed on the firing threshold of CA1 pyramidal cells [$F_{(1,53)}$ = 15.81, $p < 0.05$; $\eta^2 = 0.22$], with

morphine-treated cells firing at a more hyperpolarized potential than vehicle-treated mice (p = 0.001; Cohen's d = 0.5; Fig. 1*G*). No significant effects were noted for the smallest level of current required to elicit firing, or rheobase; however, Tat treatment tended to increase rheobase compared to Tat− controls [$F_{(1,53)}$ = 3.37, p = 0.062; η^2 = 0.06] (Fig. 1*F*). Notably, no significant differences in input resistance or capacitance were seen in pyramidal cells between any groups (Table 1).

To assess the effects of morphine withdrawal on the physiological response of CA1 pyramidal cells in mice previously exposed to morphine, vehicle-treated cells were compared separately to cells in which morphine (500 nM) was continuously present or absent (withheld) during the recordings (Fig. 1*B,D,H-J*). Analyses of the firing frequencies revealed two interactions, one between Tat and stimulus current amplitude [$F_{(15,1065)}$ = 3.47, p < 0.05; η^2 = 0.004], and another between morphine treatment and stimulus current amplitude [$F_{(15,1065)}$ = 6.43, p < 0.05; η^2 = 0.007; Fig. 1*B,D*]. *Post hoc* contrasts revealed that Tat exposure altered the firing rate of pyramidal cells depending on the amount of the stimulating current. Tat+ pyramidal cells fired at a lower frequency than Tat− neurons (p = 0.001 – 0.021; Cohen's d = 0.5 – 0.8; Fig. 1*D*) at 25 pA to 200 pA, although the firing rates did not differ at other current levels. When morphine was withheld from slices from morphine-treated mice, pyramidal cells fired at a significantly lower frequency than those in vehicle-treated mice when stimulated with 275 pA to 375 pA (p = 0.007 – 0.02; Cohen's d = 0.6 – 0.7; Fig. 1*D*). Intrinsic membrane properties were compared using two-way ANOVA. An interaction between Tat and drug treatment was observed in the resting membrane potential [$F_{(1,72)}$ = 37.99, p < 0.05; η^2 = 0.07]. Pairwise comparisons using the Bonferroni correction for multiple comparisons (significance at p < 0.008) revealed a significantly more depolarized resting membrane potential in pyramidal cells of Tat− versus Tat+ vehicle-treated mice (p = 0.003; Cohen's d = 1.2; Fig. 1*H*). Additionally, Tat-exposed pyramidal cells required a greater amount of current (rheobase) to reach their firing threshold [$F_{(1,72)}$ = 7.70, p < 0.05; η^2 = 0.10; Fig. 1*I*] and needed more current

to attain their half-maximum firing frequency (I_{50}%)—irrespective of whether morphine was present [$F_{(1,72)}$ = 6.58, p < 0.05; η^2 = 0.73] or withheld [$F_{(1,72)}$ = 4.95, p < 0.05; η^2 = 0.06; Fig. 2]. No significant effects were observed on the firing threshold of CA1 pyramidal cells (Fig. 1*J*). As in the previous comparison, neither the resistance nor capacitance were significantly affected by Tat and/or withholding morphine during the recordings (Table 1).

Morphine and Tat exposure alter the density and morphology of pyramidal cell dendritic spines within specific hippocampal layers in CA1

Distinct subsets of interneurons that project to specific pyramidal cell dendritic subdomains in discrete hippocampal layers (Pelkey et al., 2017) are a key determinant in the inhibitory-excitatory balance in CA1 (Bourne and Harris, 2011; Hiratani and Fukai, 2017). Tat perturbs distinct subsets of CA1 interneurons (Marks et al., 2016), selectively depletes Syt2-immunoreactive fibers in the SR, and suppresses long-term potentiation (Fitting et al., 2013), which were predicted to alter spine density along specific dendritic subdomains (Fig. 3). The morphological effects of Tat on CA1 pyramidal cells were previously analyzed as whole cells or larger segments without consideration to these laminar divisions (Fitting et al., 2013). To better assess the regional variations within CA1 dendritic structure, the neurons used in the electrophysiological analyses were filled with biocytin (Fig. 3*A*) and analyzed morphologically with respect to CA1 laminae (n = 10-12; Figs. 3*B-J*).

The effects of Tat and morphine on the density of dendritic spines differed in each CA1 layer. In the continued presence of morphine, there was a main effect of morphine on spine density in the SO [$F_{(1,41)}$ = 8.402, p < 0.05; η^2 = 0.17], where cells from morphine-treated mice had fewer spines per 10 µM segment (p = 0.007; Fig. 3*I*). Spine density in the SR was not affected by either morphine or Tat (Fig. 3*I*). Spine density in the SL-M was unaffected by Tat; however, in morphine-replete pyramidal cells, there was a trend for Tat to interact with morphine to increase SL-M spine density [$F_{(1,38)}$ = 3.47, p = 0.07; η^2 = 0.07]. Consequently, the

effects of morphine on SL-M spine density were examined further in pyramidal cells in Tat− and Tat+ mice separately. Significant effects were observed in Tat− cells [$t_{(19)}$ = 2.823, $p < 0.05$; η^2 = 0.29], but not Tat+ cells. Morphine-treated pyramidal cells in Tat− mice had fewer SL-M spines than in vehicle-treated Tat− mice (p = 0.015; Fig 3*K*). Furthermore, there were differences in the density of dendritic spines depending on whether morphine was present or absent during the recordings. When morphine was withheld during the recording period, a trend toward reductions in spine density was evident in the SO [$F_{(1,38)}$ = 3.64, p = 0.064; η^2 = 0.08; Fig. 3*L*] and SR [$F_{(1,38)}$ = 3.55, p = 0.067; η^2 = 0.08; Fig. 3*M*], but not the SL-M, of slices from Tat+ mice that had previously been exposed to morphine.

The morphology of dendritic spines transforms from more transient, immature thin/filopodial spines to mature mushroom spines as they become stable (Harris et al., 1992; Ochs et al., 2015; Schier et al., 2017). Representative images of dendritic spines within the major CA1 strata are shown in Fig. 4*A-C*. To unambiguously categorize dendritic spines of a morphologic type, about one half of spines with indefinite or intermediate morphology were excluded; thereby reducing the overall estimates of spine density compared to measurements in which all spines are counted (Figs. 4-5). Tat exposure reduced intermediate, stubby dendritic spine subtypes in the SO [$F_{(1,41)}$ = 6.96, p = 0.012; η^2 = 0.14; Fig. 4*E*] and SR [$F_{(1,41)}$ = 6.13; η^2 = 0.06; p = 0.018] of morphine-replete, as well as the SO [$F_{(1,40)}$ = 10.77; η^2 = 0.21; p = 0.002, Fig. 5] and SR [$F_{(1,39)}$ = 4.74; η^2 = 0.11; p = 0.036; Fig. 5] of pyramidal cells in which morphine was withheld (Fig. 5). There was a significant increase in the percentage of indefinite or intermediate spines in morphine-replete pyramidal cells in the SO [$F_{(1,37)}$ = 4.72, p = 0.0363; η^2 = 0.10; Fig. 4*E*]. Within the SR, the proportion of indefinite or intermediate spines were increased by Tat exposure in morphine-replete [$F_{(1,38)}$ = 8.11, p = 0.0071; η^2 = 0.16; Fig. 4*E*]; and morphine withheld [$F_{(1,38)}$ = 22.85, $p < 0.0001$; η^2 = 0.38; Fig. 5] pyramidal cells. Within the SL-M, withholding morphine increased the density of stubby spines compared to vehicle,

irrespective of Tat exposure [$F_{(1,36)}$ = 5.92; η^2 = 0.02; p = 0.020; Fig. 5]. Tat-exposed pyramidal cells had reduced mushroom type spines in the SR, regardless of treatment in comparisons in which morphine was withheld [$F_{(1,39)}$ = 7.37; η^2 = 0.16; p = 0.010, Fig. 5]. Continuous morphine treatment decreased thin/filopodial spines in the SR [$F_{(1,41)}$ = 6.96; η^2 = 0.14; p = 0.012; Fig. 4*E*] and SL-M [$F_{(1,37)}$ = 4.50; η^2 = 0.11; p = 0.0406; Fig. 4*E*]. Withholding morphine reduced SR thin/filopodial spine densities regardless of genotype [$F_{(1,39)}$ = 5.78; η^2 = 0.12; p = 0.021; Fig. 5]. By contrast, withholding morphine interacted to significantly alter SL-M thin/filopodial spine density only in Tat-exposed cells [$F_{(1,36)}$ = 4.32; η^2 = 0.10; p = 0.045; Fig. 5], where withholding morphine in Tat− mice, but not Tat+ mice, significantly increased the proportion of thin/filopodial spines (p = 0.029; Cohen's d = 0.9).

Morphine and Tat exposure did not alter the density of inhibitory postsynaptic puncta

To assess whether Tat-dependent reductions in specific subsets of interneurons (Marks et al., 2016) and Syt2-expressing presynaptic fibers in the SR in CA1 (Fitting et al., 2013) resulted in the loss of inhibitory postsynaptic terminals, the number of puncta was quantified along the aspinous portions of the basilar and apical dendrites of pyramidal cells as they emerged from the soma. This region of both the basilar and apical portions of the dendrite is known to have the highest percentage of inhibitory contacts onto pyramidal cells (Megıas et al., 2001). The results show no significant interactions between or main effects of either Tat or morphine on the number of inhibitory puncta within the basilar or apical dendritic shafts in the perisomatic region (Fig. 6).

CA1 volume was unaffected by morphine and Tat exposure, while Tat increased the volume of CA3

Stereology was performed to assure any changes in dendritic spine density/morphology in CA1 were not distorted by alterations in the volume in this region of the hippocampus (e.g., through gliosis, vascular leakiness (Leibrand et al., 2019), or possible disruptions in glymphatic

drainage). No significant influence of morphine or Tat genotype was observed on the volume fractions (V_V) of CA1, CA2, or the dentate gyrus. By contrast, the volume of CA3 was significantly greater among Tat+, compared to Tat−, mice irrespective of whether morphine was administered [$F_{(1,20)} = 6.350$; $\eta^2 = 0.20$; $p = 0.02$; Fig. 7; Table 2].

Morphine and Tat exposure impaired Barnes maze performance

Pyramidal neuron firing within the CA1 area of the hippocampus plays an important role in spatial memory (Gothard et al., 1996). Tat− and Tat+ mice, implanted with vehicle- or morphine-containing pellets were assessed on the Barnes maze across 4 days and a reversal probe trial (Fig. 8*A*). Compared to those implanted with vehicle pellets, mice implanted with morphine pellets took significantly longer to find the escape hole, irrespective of Tat genotype [$F_{(1,216)} = 15.15$, $p < 0.05$; $\eta^2 = 0.22$; Fig. 8*B*]. Genotype significantly interacted with the day of testing [$F_{(4,216)} = 3.60$, $p < 0.05$; $\eta^2 = 0.004$] such that Tat− mice demonstrated a significantly lower latency to escape on every day compared to their initial performance on day 1 ($p < 0.001$-0.001; Cohen's $d = 0.7 – 1.1$; Fig. 8*B*). In contrast, Tat+ mice did not outperform their initial day 1 performance until days 3 and 4 ($p < 0.001$; Cohen's $d = 0.6 – 0.7$; Fig. 7*B*). Both strains of mice demonstrated a significantly increased latency to escape on the reversal probe trial compared to their day 4 performance ($p < 0.0001$-0.003; Cohen's $d = 0.4 – 1.0$; Fig. 7*B*).

Similarly, there was a significant three-way interaction for the proportion of time spent in the correct quadrant of the Barnes maze [$F_{(4,216)} = 3.96$, $p < 0.05$; $\eta^2 = 0.05$], such that Tat+ mice spent less time in the correct quadrant than did Tat− controls on days 3 and 4 of testing ($p = 0.02$ - 0.045; Cohen's $d = 0.9$; Fig. 8*C*). Morphine did not affect the percent of time spent in the correct quadrant on days 1-4; however, on the day of reversal testing, morphine significantly increased the proportion of time spent in the correct quadrant among Tat− mice ($p = 0.01$; Cohen's $d = 0.9$), while tending to decrease it among Tat+ mice ($p = 0.056$; Cohen's $d = 0.8$; Fig. 7*C*).

The number of errors made [$F_{(1,212)} = 4.90$, $p < 0.05$; $\eta^2 = 0.08$; Fig. 8*D*] and distance traveled [$F_{(1,216)} = 9.10$, $p < 0.05$; $\eta^2 = 0.14$; Fig. 8*E*] in the Barnes maze were also significantly influenced by Tat and morphine. Tat+ mice administered morphine made more errors ($p = 0.02$; Cohen's $d = 0.4$; Fig 8*D*) and traveled greater distances on day 1 [$p = 0.02$; Cohen's $d = 0.4$; Fig. 8*E*] than did their vehicle-exposed counterparts. Conversely, morphine decreased the distance traveled by Tat− controls compared to their vehicle-exposed counterparts ($p = 0.04$; Cohen's $d = 0.4$; Fig. 8*E*). After day 1, all groups made fewer errors [$F_{(4,212)} = 22.16$, $p < 0.05$; $\eta^2 = 0.28$; Fig. 8*D*] and traveled less distance [$F_{(4,216)} = 21.91$, $p < 0.05$; $\eta^2 = 0.28$; Fig. 8*E*] on subsequent testing days ($p < 0.0001$ - 0.006; Cohen's $d = 0.1 – 1.1$). On the reversal probe trial, all groups made more errors ($p < 0.0001$; Cohen's $d = 1.2$) and traveled a greater distance ($p < 0.0001$; Cohen's $d = 1.1$) compared to their day 4 performance. Irrespective of genotype, there was a significant main effect for morphine to reduce the speed at which mice traveled [$F_{(1,216)} = 6.30$, $p < 0.05$; $\eta^2 = 0.10$; Fig. 8*F*]. The speed of travel for Tat+ animals was notably greater on the reversal probe trial compared to any other day of testing ($p < 0.0001$-0.03; Cohen's $d = 0.3 – 0.5$; Fig. 8*F*).

Discussion

The interactive effects of morphine and HIV-1 Tat were assessed on the intrinsic and evoked activity of hippocampal neurons. Changes in pyramidal cell structure and function were compared to subsequent behavioral deficits associated with neuroHIV and OUD. Morphine was delivered via subcutaneously implanted pellets, which are widely used to administer sustained, high circulating concentrations in rodents. The 25 mg implants deliver clinically relevant plasma/tissue levels of morphine (Ghazi-Khansari et al., 2006), inducing tolerance (Chefer and Shippenberg, 2009) and physical dependence within 3 d in C57BL/6 mice (Bogulavsky et al., 2009). Unlike the numerous opioid and HIV interactions in the striatum

(Fitting et al., 2020), Tat and morphine appear to act largely independently to disrupt hippocampal neuronal function. However, withholding morphine from morphine-dependent mice during *ex vivo* recordings revealed significant, albeit subtle, opioid-HIV interactions with respect to pyramidal excitability and dendritic plasticity at higher stimulating currents. Additional studies are required to determine the extent to which these responses reveal underlying neuroadaptive changes in response to sustained morphine exposure, and the extent to which the pharmacokinetics of opioid exposure mediate pathophysiological opioid and HIV interactions.

Prior observations of selective reductions in GABAergic interneuronal subpopulations (Marks et al., 2016) and reduced GABAergic SR afferents (Fitting et al., 2013) infer that Tat should, on net balance, increase neuronal excitability, as has been observed *in vitro* (Magnuson et al., 1995). However, Tat exerted the opposite effect at lower current intensities in the present study. This unanticipated decrease in CA1 pyramidal cell firing rates might result from (i) Tat-induced (and presumably transient) excitotoxic increases in GABA release from vulnerable interneurons, (ii) compensatory changes in GABAergic interneuronal networks/network oscillations (Fitting et al., 2013; Marks et al., 2016; Fitting et al., 2020), (iii) Tat-mediated increases in gephyrin, a $GABA_A$ receptor organizer (Choii and Ko, 2015; Fitting et al., 2013), and/or (iv) altered connectivity from synaptodendritic injury associated with chronic, low-level Tat exposure (Dickens et al., 2017). Tat not only disrupts the organization of excitatory and inhibitory connections impacting pyramidal cells in CA1 (Marks et al., 2016) and elsewhere in the hippocampus (Bruce-Keller et al., 2003; Maragos et al., 2003), it can also adjust inhibitory and excitatory activity through compensatory homeostatic alterations in synaptic scaling (Hargus and Thayer, 2013; Green et al., 2018). Notably, our findings identify more robust Tat-dependent deficits on CA1 pyramidal cell excitability than seen in an alternate

HIV-1 Tat transgenic mouse model (Cirino et al., 2020), which may result from more prolonged (14-day) Tat exposure.

Tat alters long term circuit neuroadaptations to morphine

In mice maintained on morphine, pyramidal cell responsiveness differed depending on whether morphine was present or withheld during the recordings. Sustained morphine exposure during the recording reduced the firing threshold but did not impact overall firing rates. By contrast, when morphine was withheld during recording, pyramidal cells had significantly lower firing rates at high stimulating currents without a commensurate change in firing threshold. Since acute morphine exposure typically increases CA1 pyramidal cell firing by inhibiting presynaptic afferents from MOR-expressing inhibitory interneurons (Siggins and Zieglgänsberger, 1981), and can hyperpolarize specific subsets of interneurons (Drake and Milner, 2002; McQuiston and Saggau, 2003; McQuiston, 2008), changes in CA1 pyramidal cell excitability following sustained morphine exposure may result from neuroadaptation due to abnormal presynaptic inhibition, changes in ion channel composition or distribution, and/or altered microcircuitry. Abruptly withholding morphine's inhibitory effects from opioid-tolerant interneurons likely results in their transient overexcitation, excess presynaptic GABA release (Christie 2008), and the suppression of pyramidal cell firing rates. When morphine was withheld from the slices taken from morphine-pelleted mice, significant reductions were seen in both (i) firing thresholds and (ii) firing frequencies at high current amplitudes, even though intrinsic resistance and capacitance measures were largely unchanged by Tat and morphine. Neuroadaptation seems to occur at multiple levels, since alterations in the number and morphologic type of dendritic spines along specific dendritic domains were also evident. Our findings are generally consistent with known circuit/ensemble-based effects of morphine on CA1 neuronal activity (Harrison et al., 2002; Liu et al., 2010; Farahmandfar et al., 2011b; Farahmandfar et al., 2011a).

Tat additionally reduced intrinsic excitability, which is also seen with prolonged Tat applications (Francesconi et al., 2018). Analysis of contrasts assessing possible morphine and Tat interactions revealed that changes in membrane potential and rheobase were largely driven by Tat. Interestingly, more protracted exposure to Tat does not alter intrinsic membrane properties despite altered excitability (Francesconi et al., 2018), suggesting the network effects of Tat precede its direct effects on CA1 pyramidal cells. However, based on morphological measures and past studies, Tat is likely affecting both the pyramidal cells and the interneuron network (Fitting et al., 2013; Marks et al., 2016; Francesconi et al., 2018).

Deficiencies in dendritic spines are associated with the severity of HAND and decreased plasticity

The development of HAND has been associated with HIV-1-induced synaptodendritic injury and culling (Ellis et al., 2007; McArthur et al., 2010; Saylor et al., 2016; Smail and Brew, 2018). Tat-induced reductions of spine density have been observed in the cortex, striatum, and hippocampus (Fitting et al., 2013; Hahn et al., 2015; Raybuck et al., 2017; Schier et al., 2017), while sustained morphine exposure is known to reduce the density of spines in CA1 pyramidal cells (Robinson et al., 2002; Zheng et al., 2010). Within the SO, we found reductions in dendritic spine density with morphine treatment, but not Tat expression. Acute morphine withdrawal also tended to reduce spine density in the SO and SR. Previously, Tat reduced the overall density of spines by 11% along the apical dendrite in Golgi-impregnated CA1 pyramidal cells (Fitting et al., 2013). The numerical differences between Golgi versus biocytin studies may reflect differences in methodology or focus since spine densities within specific hippocampal layers or morphological spine subtypes (described below) were not previously studied.

Subtle Tat and/or morphine-dependent rebalancing between excitatory and inhibitory synapses likely occurs within discrete areas of the hippocampal laminar structure, since Tat

(Marks et al., 2016) and morphine (Drake and Milner, 1999; Drake and Milner, 2002) differentially affect distinct interneuronal subpopulations having unique regional distributions. In the SL-M, morphine withdrawal increased the numbers of stubby spines regardless of Tat and decreased thin/filopodial spines along the dendrites of Tat+ mice, indicating rapid alterations in synaptic plasticity along specific regions of the dendrite. Dendritic spine stability is susceptible to inflammation (Beroun et al., 2019) and opiate- or HIV-induced alterations in NeuroD signaling (Liao et al., 2005; Zheng et al., 2010; Yuferov et al., 2013). These morphologic changes can occur rapidly, as observed in an animal model of cocaine abuse (Stankeviciute et al., 2014). Mushroom spines, which are considered the most mature/stable form, were selectively reduced in the SR following 14-d Tat exposure. While the SR receives input from Shaffer collaterals, the SL-M receive distinct inputs of differentially processed spatial and non-spatial sensory information from the entorhinal cortex via the temporoammonic and perforant path fibers. The putative integrative mechanism formed by the interneuron network and pyramidal cells in CA1 can easily be unbalanced, leading to memory formation dysfunction (Kitamura et al., 2014; Kitamura et al., 2015; Marks et al., 2016; Marks et al., 2020). Although our findings show no differences in gephyrin puncta within pyramidal cell dendrites near the soma (Fig. 7), previously demonstrated increases in gephyrin levels do not discriminate pyramidal cells from other CA1 neuron types (Fitting et al., 2013). Selective spine losses in combination with disruptions to the inhibitory interneuron network (Fitting et al., 2013; Marks et al., 2016) are likely to contribute to decreased LTP (Bao et al., 2007; Fitting et al., 2013) and the altered CA1 pyramidal cell structure and function seen here.

Morphine and Tat disrupt spatial memory

HIV-1 Tat has previously been shown to attenuate spatial memory in the Barnes maze task (Carey et al., 2012; Kesby et al., 2016; Marks et al., 2016). Tat-mediated impairment of spatial memory coincided with reductions in pyramidal cell excitability at lower stimulating

currents in the present study. Morphine treatment counteracted some of the negative effects of Tat, such as the proportion of time spent in incorrect quadrants but exacerbated the number of errors made by Tat+ mice on a reversal probe trial and greatly increased the latency for all mice to find the escape hole. These findings may reveal cognitive distinctions between morphine's effects to potentially preserve aspects of Tat-impaired reference memory, while impeding novel search strategies. The notion that Tat and morphine can independently impair spatial memory is consistent with the minimal behavioral interactions observed in the current study (Zhu et al., 2011; Kitanaka et al., 2015; Kesby et al., 2016; Marks et al., 2016). Opioid-dependent individuals reportedly demonstrate hyper-connectivity in hippocampo-amygdalar memory circuits that may promote the recall of drug-associated cues (Zhang et al., 2017; Ma et al., 2020). This hyperactive associative circuitry may counterbalance the general effects of Tat (Basu and Siegelbaum, 2015; Roy et al., 2017; Sharifi et al., 2020).

The morphine implants used result in relatively high plasma levels, like those seen in OUD in which tolerance to high opioid dosages is typical. Higher morphine doses can generate a biphasic response in which activity oscillates before returning to baseline (Vasko and Domino, 1978). Tolerance to morphine's depressive effects develops more rapidly than to its stimulatory effects (Vasko and Domino, 1978; Ling et al., 1989; Le Marec et al., 2011), raising the possibility of locomotor confounds. In the present study, morphine treatment reduced overall velocity and initial distance traveled among Tat- mice, but increased distance traveled by Tat+ mice. Differences in the distance traveled were not evident after day 1, but we cannot rule out the contribution of motor influences given the high dose of morphine used in the present study—particularly during the first few days of exposure, while mice are still developing tolerance to the drug.

The collective findings suggest that the structure and function of CA1 pyramidal cells are dramatically influenced by morphine exposure. The presence of an additional stressor

610 such as Tat may enhance the destabilizing effects of fluctuating morphine levels. While the
611 striatum tends to display additive or synergistic interactions, Tat and morphine acted more
612 independently and occasionally seemed to counteract each other in the hippocampus. Rapid
613 alterations in pyramidal cell structure and function in response to opiate withdrawal
614 underscore the potential importance of opiate pharmacokinetics and the sustained
615 consequences of fluctuating drug levels (as seen in OUD) in driving the pathobiology of opiate
616 abuse-neuroHIV comorbidity. The nuanced regional effects of HIV and opioid drugs open
617 exciting questions on the extent to which network level effects on behavioral dysfunction are
618 driven by the unique interplay of pathological interactions and counteractive processes in
619 distinct brain regions, and whether the counteractive effects can be utilized as a treatable
620 target.

Figure Legends

Figure 1. Analysis of the firing frequency of CA1 pyramidal cells from Tat– or Tat+ mice treated with vehicle or morphine time-release implants in which morphine is present (500 nM) or withheld (0 nM) during the recordings. ***A,B,*** Representative traces are depicted at the 100 and 350 pA current steps in which morphine (Morph) is present (500 nM) (***A***) or withheld (0 nM) (***B***) during the recordings. ***A,C,*** Pyramidal cell firing rates were unaffected by sustained morphine exposure. ***B,D,*** By contrast, when morphine was withheld during recordings from mice previously maintained on morphine, firing rates were significantly suppressed. ***C,*** CA1 pyramidal cells from Tat+ mice fired at a lower frequency than those of Tat− mice between 50 and 150 pA, but were unaffected by exposure to morphine during recordings (***C***). ***C,D,*** Tat genotype interacted with the amount of current applied. ***D,*** Withholding morphine from slices isolated from morphine-exposed mice resulted in significantly lower pyramidal cell firing rates at stimulating currents from 275 pA to 375 pA compared to morphine-naïve cells ($^{\dagger}p < 0.05$); nevertheless, Tat and morphine did not interact statistically perhaps because the effect of withholding morphine was not seen at other stimulating currents and at 25 pA-200 pA current steps in pyramidal cells from Tat+ mice had lower firing rates than those from Tat− mice. ***E,*** Resting membrane potential (V_R) showed significant interactions when exposed to Tat or morphine. Tat+ neurons were significantly more depolarized at rest, while morphine treatment appeared to negate the effects of Tat. ***F,*** While no significant effects were noted in rheobase, there was a trend ($p = 0.06$) for pyramidal cells from Tat+ mice to require a greater amount of current to reach a threshold for firing compared to cells from Tat− mice. ***G,*** The threshold for firing (mV) is significantly reduced in cells from morphine-treated mice. ***H,*** There was a significant interaction between Tat and morphine on resting membrane potential (V_R), which resulted from greater depolarized membrane potentials in vehicle-treated Tat+ mice. ***I,*** Tat significantly increased rheobase—irrespective of prior morphine treatment during the recording

of morphine-replete slices. Pyramidal cells from Tat+ mice required a greater amount of current (pA) to reach the threshold potential for firing than Tat− mice, even though the firing threshold (mV) of CA1 pyramidal cells was unaffected by Tat or morphine exposure (***J***). Patched cells were stimulated with 500 ms current pulses starting at −100 pA and escalating to 400 pA in 25 pA steps. * indicates significant difference between Tat− and Tat+ tissues; † indicates a significant decline in firing rates in slices from Tat+, but not Tat−, mice previously exposed to morphine when morphine was withheld ($p < 0.05$).

Figure 2. The amount of current injected to maintain half-maximum firing frequency (I_{50}%), or 50% of the maximal firing rate observed across all current steps (−100 to 400 pA in 25 pA steps) per cell (Fig 2 A-D), is significantly increased in CA1 pyramidal cells of Tat+ compared to Tat− mice [main effect; $F_{(1,72)} = 7.70$; $p < 0.05$]—irrespective of whether morphine is present or withheld during the recording. These data indicate that one week of Tat exposure is sufficient to fundamentally alter CA1 pyramidal cell excitability. * indicates a significant difference between pyramidal cells from Tat− and Tat+ mice ($p < 0.05$); individual data points, representing individual cells, are shown by open circles.

Figure 3. Effects of Tat and morphine on spine density along specific pyramidal cell dendritic segments within the stratum oriens (SO), stratum radiatum (SR), and stratum lacunosum moleculare (SL-M) of hippocampal area CA1. ***A,*** Reconstructed Z-stack image of a representative biocytin-filled pyramidal cell within hippocampal area CA1 from a vehicle-treated Tat− mouse. ***B-E,*** Sample pyramidal cell dendritic segments and 3-D reconstructions from the SO of control, morphine, Tat, and morphine plus Tat-exposed mice. The top image is the raw image file (***B-E***). The image below shows a representative 3D-reconstructed dendritic segment

(*green*) and its associated spines (*blue*) (***B'-E'***). The final image superimposes the raw image of the dendrite and its spines with the 3D-reconstruction of the same dendritic segment and spines (***B''-E''***). Scale bar = 50 μM. ***F,I,L,*** Illustration of the location of pyramidal cell dendritic portion sampled is shaded in gray (***F***) and mean spine densities ± the SEM within the SO (***I,L***). ***I,*** There was a main effect of sustained morphine exposure *in vivo* and during recordings to reduce overall SO spine density ($^{\dagger}p = 0.007$). ***L,*** Spine losses were no longer significant after morphine was withheld—suggesting morphine-dependent spines losses are plastic and reversible. ***G,J,M,*** Illustration of the location of pyramidal cell dendritic portion sampled is shaded in gray (***G***) and mean spine densities ± the SEM within the SR (***J,M***). ***J,*** No differences in spine density in SR dendrites were observed in Tat− or Tat+ in the absence or presence of sustained exposure to morphine *in vivo* and during recordings *ex vivo.* ***M,*** By contrast, withholding morphine tended to induce spine losses. ***H,K,N,*** Illustration of the location of pyramidal cell dendritic portion sampled is shaded in gray (***H***) and mean spine densities ± the SEM within the SL-M (***K,N***). ***K,*** Morphine caused a reduction in SL-M dendritic spine density in pyramidal cells from Tat−, but not Tat+, mice (***$p < 0.05$). In fact, there was a trend for Tat to reverse morphine-dependent reductions in dendritic spine density with sustained morphine exposure *ex vivo*, albeit not significant ($p = 0.07$), suggesting that Tat and morphine uniquely interact to increase spine numbers on the SL-M (***G***). ***N,*** By contrast, withholding morphine from *ex vivo* slices during recordings negated any changes in spine density seen when morphine is present (***N*** vs. ***K***)—suggesting the changes in spine density caused by morphine are highly plastic and modifiable.

Figure 4. ***A-F,*** Spine subtype analyses of CA1 pyramidal neurons cells from Tat– or Tat+ mice. Mice were treated with vehicle control or morphine (25 mg) time-release implants; during electrophysiological recordings, morphine was present (500 nM, "morphine"). Spine subtypes

696 ("mushroom", "stubby", or "thin/filopodial") were analyzed individually. Dendritic spines of an
697 indefinite or intermediate morphology were-analyzed separately, thereby reducing the overall
698 estimates of spine density compared to measurements in which all spines are counted (Fig. 3).
699 Tat exposure reduced intermediate, stubby dendritic spine subtypes in the SO and SR of
700 morphine-replete pyramidal cells. There was a significant increase in the percentage of
701 indefinite or intermediate spines in pyramidal cells in the SO with sustained morphine exposure.
702 Within the SR, the proportion of indefinite or intermediate spines were increased in Tat-
703 exposed pyramidal cells continuously exposed to morphine. Continuous morphine treatment
704 decreased thin/filopodial spines in the SR and SL-M, while increasing in Tat exposed cells. *
705 indicates significant difference between Tat− and Tat+ tissues; † indicates significant difference
706 between morphine-replete and vehicle-treated tissues, $p < 0.05$.
707
708 **Figure 5.** Spine subtype analyses of CA1 pyramidal neurons cells from Tat– or Tat+ mice.
709 Mice previously treated with vehicle control or morphine (25 mg) time-release implants in which
710 morphine was withheld (0 nM, "withheld") during electrophysiological recordings. Spine
711 subtypes ("mushroom", "stubby", or "thin/filopodial") were analyzed individually. Dendritic
712 spines of an indefinite or intermediate morphology were analyzed separately, thereby reducing
713 the overall estimates of spine density compared to measurements in which all spines are
714 counted (Fig. 3). Tat exposure reduced intermediate, stubby dendritic spine subtypes in the
715 SO and SR of pyramidal cells in which morphine was withheld. Within the SR, withholding
716 morphine increased the proportion of indefinite spines with concurrent Tat exposure. In the SL-
717 M, morphine treatment increased the density of stubby spines when morphine was withheld,
718 irrespective of Tat exposure. Tat exposure reduced mushroom type spines in the SR
719 regardless of treatment. Withholding morphine reduced SR thin/filopodial spine densities
720 regardless of genotype. By contrast, withholding morphine interacted to significantly alter SL-M
721 thin/filopodial spine density in Tat-exposed pyramidal cells, while withholding morphine

722 specifically increased the proportion of thin/filopodial spines in Tat− mice. * indicates significant
723 difference between Tat− and Tat+ tissues; † indicates significant difference between vehicle-
724 treated and morphine-withheld tissues, $p < 0.05$.

725

726 **Figure 6.** Assessment of inhibitory, postsynaptic gephyrin puncta within the aspinous, proximal
727 dendrites of CA1 pyramidal cells. Biocytin-filled pyramidal cells labeled with an Alexa 594-
728 conjugated streptavidin probe (*red*) and gephyrin puncta (*green*) were analyzed. (***A,B,B'***), A
729 third channel (*blue—with darker blue puncta are in front of the dendrite; lighter blue puncta are*
730 *behind the dendrite*) (***B,B'***), only identifying the gephyrin puncta that were adjacent or
731 overlapped with the aspinous portions of the basilar (***C***) or perisomatic apical (***D***) pyramidal cell
732 dendrite, from 3-D reconstructed images was quantified**.** No changes in the number of
733 gephyrin-immunoreactive puncta were observed. Data represent the mean number of
734 gephyrin-positive puncta ± SEM per 10 µM length of dendrite.

735

736 **Figure 7.** ***A,B,*** There was no effect of Tat or morphine exposure on the volume fraction (V_V) of
737 hippocampal areas CA1, CA2, or the dentate gyrus; however, the volume of CA3 was
738 significantly increased by Tat induction irrespective of morphine exposure (see Table 1).
739 Importantly, the measurements of dendritic spine density (Figs. 4 & 5) were not distorted by
740 morphine- or Tat-dependent alterations in the volume of hippocampal area CA1. Images show
741 representative Hoechst 33342-stained, 40 µm coronal sections of the hippocampus from Tat−
742 (***A***) and Tat+ (***B***) mice used for stereology.

743

744 **Figure 8.** Effects of morphine and HIV-1 Tat exposure on spatial learning. ***A,*** Representative
745 paths traveled by vehicle- or morphine-exposed Tat− and Tat+ mice (*n* = 12-17/group) on the
746 Barnes Maze test (*the filled black circle indicates the escape goal; open circles indicate decoy*
747 *escape locations*). ***B,*** Tat− mice showed a significant decrease in the latency (s) during four
748 days of training trials to find the escape hole compared to Tat+ mice, while morphine increased
749 the latency irrespective of genotype. ***C,*** Tat− mice spent a greater proportion of time in the
750 correct quadrant than Tat+ mice. Although morphine increased the proportion of time in Tat+
751 mice spent in the correct quadrant, morphine-treated mice spent significantly less time in the
752 correct quadrant during the reversal probe trial. ***D,*** Tat− and Tat+ mice made fewer errors on
753 days 3 and 4. Morphine increased the errors made by Tat+ mice on the reversal probe trials. ***E,***
754 Tat+ mice traveled shorter distances (cm) on days 1 and 2 and reduced their daily travel
755 significantly faster than Tat− mice. On day 1, morphine increased the distance traveled by Tat+
756 mice, while reducing the distance traveled by Tat− mice. ***F,*** The velocity of travel (cm/s) was
757 reduced by morphine exposure. † main effect for morphine to differ from vehicle treatments; $^{\shortparallel}$
758 reversal day performance significantly differs from day 4 performance; $^{+}$ indicates the group
759 significantly differs from day 1 performance; * indicates the Tat− and respective Tat+ groups
760 differ significantly; ‡ indicates the morphine and respective vehicle-treated groups differ
761 significantly, $p < 0.05$.

762

763 **Table 1. Membrane properties of CA1 pyramidal cells after exposure to Tat and morphine**

***In vivo* treatment**	**Tat− Vehicle *n* = 13**	**Tat+ Vehicle *n* = 12**	**Tat− Morphine *n* = 19**	**Tat+ Morphine *n* = 13**	**Tat− Morphine *n* = 29**	**Tat+ Morphine *n* = 22**
***Ex vivo* treatment**	**—**	**—**	morphine	morphine	**—**	**—**
Capacitance (pF)	130.2 ± 12.4	175.4 ± 16.0	157.7 ± 9.5	138.4 ± 10.3	166.3 ± 8.8	184.7 ± 13.5
Resistance (MΩ)	182.1 ± 21.6	154.7 ± 16.9	146.4 ± 10.2	127.2 ± 8.9	179.0 ± 10.9	149.2 ± 16.2

764

765 Capacitance and resistance values from pyramidal cell recordings from Tat− and Tat+ mice
766 maintained on vehicle- (control) or morphine- (25 mg) containing time-release implants in which
767 morphine (500 nM) was present ('morphine') or withheld (**—**) during recordings in hippocampal
768 slices *ex vivo*. No significant changes were observed. All values are shown as mean ± SEM.

Table 2. Stereological analyses of hippocampal volume.

	Tat−		Tat+	
	Vehicle	Morphine (25 mg)	Vehicle	Morphine (25 mg)
CA1	44.35 ± 2.48 %	43.97 ± 0.72 %	40.19 ± 3.48 %	46.13 ± 3.18 %
CA2	5.00 ± 0.71 %	5.03 ± 0.68 %	4.70 ± 0.65 %	5.21 ± 1.07 %
CA3	26.71 ± 1.93 %	26.58 ± 1.53 %	**35.92 ± 2.26 % ***	**28.91 ± 2.88 % ***
DG	26.94 ± 1.45 %	24.42 ± 1.24 %	28.31 ± 2.19 %	28.07 ± 2.87 %

No significant alterations in total hippocampal volume for CA1 were found in male Tat transgenic mice (n = 5-8) following 2 weeks of doxycycline and 5 d subcutaneous vehicle- or morphine- (25 mg) containing time-release implant. A significant increase in hippocampal area CA3 volume was detected for Tat+ mice. * indicates a significant difference between Tat− and Tat+ tissues, $p < 0.05$.

776 References
777
778 Anthony IC, Norrby KE, Dingwall T, Carnie FW, Millar T, Arango JC, Robertson R, Bell JE
779 (2010) Predisposition to accelerated Alzheimer-related changes in the brains of human
780 immunodeficiency virus negative opiate abusers. Brain 133:3685-3698.

781 Bao G, Kang L, Li H, Li Y, Pu L, Xia P, Ma L, Pei G (2007) Morphine and heroin differentially
782 modulate in vivo hippocampal LTP in opiate-dependent rat. Neuropsychopharmacology
783 32:1738-1749.

784 Barnes CA (1979) Memory deficits associated with senescence: a neurophysiological and
785 behavioral study in the rat. J Comp Physiol Psychol 93:74-104.

786 Basu J, Siegelbaum SA (2015) The corticohippocampal circuit, synaptic plasticity, and memory.
787 Cold Spring Harbor perspectives in biology 7:a021733.

788 Beroun A, Mitra S, Michaluk P, Pijet B, Stefaniuk M, Kaczmarek L (2019) MMPs in learning and
789 memory and neuropsychiatric disorders. Cell Mol Life Sci 76:3207-3228.

790 Bogulavsky JJ, Gregus AM, Kim PT, Costa AC, Rajadhyaksha AM, Inturrisi CE (2009) Deletion
791 of the glutamate receptor 5 subunit of kainate receptors affects the development of morphine
792 tolerance. J Pharmacol Exp Ther 328:579-587.

793 Boraud T, Vassileva J, Ahn W-Y, Weber KM, Busemeyer JR, Stout JC, Gonzalez R, Cohen MH
794 (2013) Computational modeling reveals distinct effects of HIV and history of drug use on
795 decision-making processes in women. PLoS ONE 8:e68962.

796 Borjkhani M, Bahrami F, Janahmadi M (2018) Computational modeling of opioid-induced
797 synaptic plasticity in hippocampus. PLoS One 13:e0193410.

798 Bourne JN, Harris KM (2011) Coordination of size and number of excitatory and inhibitory
799 synapses results in a balanced structural plasticity along mature hippocampal CA1 dendrites
800 during LTP. Hippocampus 21:354-373.

801 Bruce-Keller AJ, Chauhan A, Dimayuga FO, Gee J, Keller JN, Nath A (2003) Synaptic transport
802 of human immunodeficiency virus-Tat protein causes neurotoxicity and gliosis in rat brain. J
803 Neurosci 23:8417-8422.

804 Bruce-Keller AJ, Turchan-Cholewo J, Smart EJ, Geurin T, Chauhan A, Reid R, Xu R, Nath A,
805 Knapp PE, Hauser KF (2008) Morphine causes rapid increases in glial activation and
806 neuronal injury in the striatum of inducible HIV-1 Tat transgenic mice. Glia 56:1414-1427.

807 Byrd D, Murray J, Safdieh G, Morgello S (2012) Impact of opiate addiction on
808 neuroinflammation in HIV. J Neurovirol 18:364-373.

809 Byrd DA, Fellows RP, Morgello S, Franklin D, Heaton RK, Deutsch R, Atkinson JH, Clifford DB,
810 Collier AC, Marra CM, Gelman B, McCutchan JA, Duarte NA, Simpson DM, McArthur J,
811 Grant I (2011) Neurocognitive impact of substance use in HIV infection. J Acquir Immune
812 Defic Syndr 58:154-162.

Calhoun ME, Kurth D, Phinney AL, Long JM, Hengemihle J, Mouton PR, Ingram DK, Jucker M (1998) Hippocampal neuron and synaptophysin-positive bouton number in aging C57BL/6 mice. Neurobiol Aging 19:599-606.

Camara ML, Corrigan F, Jaehne EJ, Jawahar MC, Anscomb H, Koerner H, Baune BT (2013) TNF-alpha and its receptors modulate complex behaviours and neurotrophins in transgenic mice. Psychoneuroendocrinology 38:3102-3114.

Campbell EM et al. (2017) Detailed transmission network analysis of a large opiate-driven outbreak of HIV infection in the United States. J Infect Dis 216:1053-1062.

Carey AN, Sypek EI, Singh HD, Kaufman MJ, McLaughlin JP (2012) Expression of HIV-Tat protein is associated with learning and memory deficits in the mouse. Behav Brain Res 229:48-56.

Chefer VI, Shippenberg TS (2009) Augmentation of morphine-induced sensitization but reduction in morphine tolerance and reward in delta-opioid receptor knockout mice. Neuropsychopharmacology 34:887-898.

Christie MJ (2008) Cellular neuroadaptations to chronic opioids: tolerance, withdrawal and addiction. Br J Pharmacol 154:384-396.

Choii G, Ko J (2015) Gephyrin: a central GABAergic synapse organizer. Exp Mol Med 47:e158.

Cirino TJ, Harden SW, McLaughlin JP, Frazier CJ (2020) Region-specific effects of HIV-1 Tat on intrinsic electrophysiological properties of pyramidal neurons in mouse prefrontal cortex and hippocampus. J Neurophysiol 123: 1332-1341.

Crawley JN, Paylor R (1997) A proposed test battery and constellations of specific behavioral paradigms to investigate the behavioral phenotypes of transgenic and knockout mice. Hormones and behavior 31:197-211.

Denis CM, Morales KH, Wu Q, Metzger DS, Cheatle MD (2019) Association between diagnoses of chronic noncancer pain, substance use disorder, and HIV-related outcomes in people living with HIV. J Acquir Immune Defic Syndr 82 Suppl 2:S142-S147.

Dickens AM, Yoo SW, Chin AC, Xu J, Johnson TP, Trout AL, Hauser KF, Haughey NJ (2017) Chronic low-level expression of HIV-1 Tat promotes a neurodegenerative phenotype with aging. Scientific reports 7:7748.

Drake CT, Milner TA (1999) Mu opioid receptors are in somatodendritic and axonal compartments of GABAergic neurons in rat hippocampal formation. Brain Res 849:203-215.

Drake CT, Milner TA (2002) Mu opioid receptors are in discrete hippocampal interneuron subpopulations. Hippocampus 12:119-136.

Ellis R, Langford D, Masliah E (2007) HIV and antiretroviral therapy in the brain: neuronal injury and repair. Nature reviews Neuroscience 8:33-44.

848 Farahmandfar M, Zarrindast MR, Kadivar M, Karimian SM, Naghdi N (2011a) The effect of
849 morphine sensitization on extracellular concentrations of GABA in dorsal hippocampus of
850 male rats. Eur J Pharmacol 669:66-70.

851 Farahmandfar M, Karimian SM, Zarrindast MR, Kadivar M, Afrouzi H, Naghdi N (2011b)
852 Morphine sensitization increases the extracellular level of glutamate in CA1 of rat
853 hippocampus via mu-opioid receptor. Neurosci Lett 494:130-134.

854 Fauci AS, Redfield RR, Sigounas G, Weahkee MD, Giroir BP (2019) Ending the HIV epidemic:
855 a plan for the United States. JAMA 321:844-845.

856 Fitting S, Knapp PE, Zou S, Marks WD, Bowers MS, Akbarali HI, Hauser KF (2014) Interactive
857 HIV-1 Tat and morphine-induced synaptodendritic injury is triggered through focal
858 disruptions in Na^+ influx, mitochondrial instability, and Ca^{2+} overload. J Neurosci 341:12850-
859 12864.

860 Fitting S, McRae M, Hauser KF (2020) Opioid and neuroHIV Comorbidity – Current and Future
861 Perspectives. J Neuroimmune Pharm. 15(4):584-627.

862 Fitting S, Ngwainmbi J, Kang M, Khan FA, Stevens DL, Dewey WL, Knapp PE, Hauser KF,
863 Akbarali HI (2015) Sensitization of enteric neurons to morphine by HIV-1 Tat protein.
864 Neurogastroenterology & Motility 27:468-480.

865 Fitting S, Stevens DL, Khan FA, Scoggins KL, Enga RM, Beardsley PM, Knapp PE, Dewey WL,
866 Hauser KF (2016) Morphine Tolerance and Physical Dependence Are Altered in Conditional
867 HIV-1 Tat Transgenic Mice. J Pharmacol Exp Ther 356:96-105.

868 Fitting S, Ignatowska-Jankowska BM, Bull C, Skoff RP, Lichtman AH, Wise LE, Fox MA, Su J,
869 Medina AE, Krahe TE, Knapp PE, Guido W, Hauser KF (2013) Synaptic dysfunction in the
870 hippocampus accompanies learning and memory deficits in human immunodeficiency virus
871 type-1 Tat transgenic mice. Biol Psychiatry 73:443-453.

872 Fitting S, Xu R, Bull C, Buch SK, El-Hage N, Nath A, Knapp PE, Hauser KF (2010) Interactive
873 Comorbidity between Opioid Drug Abuse and HIV-1 Tat. Am J Pathol 17:1397-1410.

874 Fitting S, Zou S, Chen W, Vo P, Hauser KF, Knapp PE (2010) Regional Heterogeneity and
875 Diversity in Cytokine and Chemokine Production by Astroglia: Differential Responses to HIV-
876 1 Tat, gp120, and Morphine Revealed by Multiplex Analysis. J Proteome Res 9:1795-1804.

877 Francesconi W, Berton F, Marcondes MCG (2018) HIV-1 Tat alters neuronal intrinsic
878 excitability. BMC Research Notes 11:275.

879 Ghazi-Khansari M, Zendehdel R, Pirali-Hamedani M, Amini M (2006) Determination of
880 morphine in the plasma of addicts in using Zeolite Y extraction following high-performance
881 liquid chromatography. Clinica Chimica Acta 364:235-238.

882 Gothard KM, Skaggs WE, Moore KM, McNaughton BL (1996) Binding of hippocampal CA1
883 neural activity to multiple reference frames in a landmark-based navigation task. J Neurosci
884 16:823-835.

885 Green MV, Raybuck JD, Zhang X, Wu MM, Thayer SA (2018) Scaling Synapses in the
886 Presence of HIV. Neurochem Res 44(1):234-246.

887 Hahn YK, Paris JJ, Lichtman AH, Hauser KF, Sim-Selley LJ, Selley DE, Knapp PE (2015)
888 Central HIV-1 Tat exposure elevates anxiety and fear conditioned responses of male mice
889 concurrent with altered μ-opioid receptor-mediated G-protein activation and β-arrestin 2
890 activity in the forebrain. Neurobiol Dis 92:124-136.

891 Hahn YK, Podhaizer EM, Farris SP, Miles MF, Hauser KF, Knapp PE (2015) Effects of chronic
892 HIV-1 Tat exposure in the CNS: heightened vulnerability of males versus females to
893 changes in cell numbers, synaptic integrity, and behavior. Brain Struct Func 220:605-623.

894 Hargus NJ, Thayer SA (2013) Human immunodeficiency virus-1 Tat protein increases the
895 number of inhibitory synapses between hippocampal neurons in culture. J Neurosci
896 33:17908-17920.

897 Harris KM, Jensen FE, Tsao B (1992) Three-dimensional structure of dendritic spines and
898 synapses in rat hippocampus (CA1) at postnatal day 15 and adult ages: implications for the
899 maturation of synaptic physiology and long-term potentiation. J Neurosci 12:2685-2705
900 [**erratum:** J Neurosci (1992) 12:following table of contents].

901 Harrison JM, Allen RG, Pellegrino MJ, Williams JT, Manzoni OJ (2002) Chronic Morphine
902 Treatment Alters Endogenous Opioid Control of Hippocampal Mossy Fiber Synaptic
903 Transmission. J Neurophysiol 87:2464-2470.

904 Hauser KF, Fitting S, Dever SM, Podhaizer EM, Knapp PE (2012) Opiate drug use and the
905 pathophysiology of neuroAIDS. Curr HIV Res 10:435-452.

906 Hiratani N, Fukai T (2017) Detailed dendritic excitatory/inhibitory balance through
907 heterosynaptic spike-timing-dependent plasticity. J Neurosci 37:12106-12122.

908 Kesby JP, Markou A, Semenova S, Group T (2016) Effects of HIV/TAT protein expression and
909 chronic selegiline treatment on spatial memory, reversal learning and neurotransmitter levels
910 in mice. Behav Brain Res 311:131-140.

911 Keutmann MK, Gonzalez R, Maki PM, Rubin LH, Vassileva J, Martin EM (2017) Sex
912 differences in HIV effects on visual memory among substance-dependent individuals.
913 Journal of clinical and experimental neuropsychology 39:574-586.

914 Kitamura T, Sun C, Martin J, Kitch LJ, Schnitzer MJ, Tonegawa S (2015) Entorhinal cortical
915 ocean cells encode specific contexts and drive context-specific fear memory. Neuron
916 87:1317-1331.

917 Kitamura T, Pignatelli M, Suh J, Kohara K, Yoshiki A, Abe K, Tonegawa S (2014) Island cells
918 control temporal association memory. Science 343:896-901.

919 Kitanaka J, Kitanaka N, Hall FS, Fujii M, Goto A, Kanda Y, Koizumi A, Kuroiwa H, Mibayashi S,
920 Muranishi Y, Otaki S, Sumikawa M, Tanaka K, Nishiyama N, Uhl GR, Takemura M (2015)
921 Memory impairment and reduced exploratory behavior in mice after administration of
922 systemic morphine. J Exp Neurosci 9:27-35.

923 Kovacs GG, Horvath MC, Majtenyi K, Lutz MI, Hurd YL, Keller E (2015) Heroin abuse
924 exaggerates age-related deposition of hyperphosphorylated tau and p62-positive inclusions.
925 Neurobiol Aging 36:3100-3107.

926 Kreek MJ (1987) Tolerance and dependence: implications for the pharmacological treatment of
927 addiction. NIDA Res Monogr 76:53-62.

928 Kreek MJ (2001) Drug addictions. Molecular and cellular endpoints. Ann N Y Acad Sci
929 937:2749.

930 Kreek MJ, LaForge KS, Butelman E (2002) Pharmacotherapy of addictions. Nat Rev Drug
931 Discov 1:710-726.

932 Krogh KA, Lyddon E, Thayer SA (2015) HIV-1 Tat activates a RhoA signaling pathway to
933 reduce NMDA-evoked calcium responses in hippocampal neurons via an actin-dependent
934 mechanism. J Neurochem 132:354-366.

935 Leibrand CR, Paris JJ, Jones AM, Masuda QN, Halquist MS, Kim WK, Knapp PE, Kashuba
936 ADM, Hauser KF, McRae M (2019) HIV-1 Tat and opioids act independently to limit
937 antiretroviral brain concentrations and reduce blood-brain barrier integrity. J Neurovirol
938 25:560-577.

939 Le Marec T, Marie-Claire C, Noble F, Marie N (2011) Chronic and intermittent morphine
940 treatment differently regulates opioid and dopamine systems: a role in locomotor
941 sensitization. Psychopharmacology (Berl) 216:297-303.

942 Lerner AM, Fauci AS (2019) Opioid Injection in Rural Areas of the United States. Jama 322.

943 Li ST, Matsushita M, Moriwaki A, Saheki Y, Lu YF, Tomizawa K, Wu HY, Terada H, Matsui H
944 (2004) HIV-1 Tat inhibits long-term potentiation and attenuates spatial learning [corrected].
945 Ann Neurol 55:362-371.

946 Li W, Li Q, Wang Y, Zhu J, Ye J, Yan X, Li Y, Chen J, Liu J, Li Z, Wang W, Liu Y (2016)
947 Methadone-induced damage to white matter integrity in methadone maintenance patients: a
948 longitudinal self-control DTI Study. Sci Rep 6:19662.

949 Liao D, Lin H, Law PY, Loh HH (2005) Mu-opioid receptors modulate the stability of dendritic
950 spines. Proc Natl Acad Sci U S A 102:1725-1730.

951 Ling GS, Paul D, Simantov R, Pasternak GW (1989) Differential development of acute
952 tolerance to analgesia, respiratory depression, gastrointestinal transit and hormone release
953 in a morphine infusion model. Life Sci 45:1627-1636.

954 Liu F, Jiang H, Zhong W, Wu X, Luo J (2010) Changes in ensemble activity of hippocampus
955 CA1 neurons induced by chronic morphine administration in freely behaving mice. Neurosci
956 171:747-759.

957 Lucas GM, Gebo KA, Chaisson RE, Moore RD (2002) Longitudinal assessment of the effects of
958 drug and alcohol abuse on HIV-1 treatment outcomes in an urban clinic. AIDS 16:767-774.

959 Ma Q, Fu Y, Cao Z, Shao D, Song J, Sheng H, Yang L, Cui D, Chen M, Zhao F, Luo MH, Lai B,
960 Zheng P (2020) A Conditioning-strengthened circuit from CA1 of dorsal hippocampus to
961 basolateral amygdala participates in morphine-withdrawal memory retrieval. Front Neurosci
962 14:646.

963 Magnuson DS, Knudsen BE, Geiger JD, Brownstone RM, Nath A (1995) Human
964 immunodeficiency virus type 1 tat activates non-*N*-methyl-D- aspartate excitatory amino acid
965 receptors and causes neurotoxicity. Ann Neurol 37:373-380.

966 Maki PM, Cohen MH, Weber K, Little DM, Fornelli D, Rubin LH, Perschler P, Gould F, Martin E
967 (2009) Impairments in memory and hippocampal function in HIV-positive vs HIV-negative
968 women: a preliminary study. Neurology 72:1661-1668.

969 Maragos WF, Tillman P, Jones M, Bruce-Keller AJ, Roth S, Bell JE, Nath A (2003) Neuronal
970 injury in hippocampus with human immunodeficiency virus transactivating protein, Tat.
971 Neuroscience 117:43-53.

972 Marks WD, Yamamoto N, Kitamura T (2020) Complementary roles of differential medial
973 entorhinal cortex inputs to the hippocampus for the formation and integration of temporal and
974 contextual memory (Systems Neuroscience). Eur J Neurosci. doi: 10.1111/ejn.14737.

975 Marks WD, Paris JJ, Schier CJ, Denton MD, Fitting S, McQuiston AR, Knapp PE, Hauser KF
976 (2016) HIV-1 Tat causes cognitive deficits and selective loss of parvalbumin, somatostatin,
977 and neuronal nitric oxide synthase expressing hippocampal CA1 interneuron
978 subpopulations. J Neurovirol 22:747-762.

979 McArthur JC, Steiner J, Sacktor N, Nath A (2010) Human immunodeficiency virus-associated
980 neurocognitive disorders: Mind the gap. Ann Neurol 67:699-714.

981 McQuiston AR (2007) Effects of mu-opioid receptor modulation on $GABA_B$ receptor synaptic
982 function in hippocampal CA1. J Neurophysiol 97:2301-2311.

983 McQuiston AR (2008) Layer selective presynaptic modulation of excitatory inputs to
984 hippocampal cornu Ammon 1 by mu-opioid receptor activation. Neuroscience 151:209-221.

985 McQuiston AR, Saggau P (2003) Mu-opioid receptors facilitate the propagation of excitatory
986 activity in rat hippocampal area CA1 by disinhibition of all anatomical layers. J Neurophysiol
987 90:1936-1948.

988 Megıas M, Emri Z, Freund TF, Gulyás AI (2001) Total number and distribution of inhibitory and´
989 excitatory synapses on hippocampal CA1 pyramidal cells. Neuroscience 102:527-540.

990 Meyer VJ, Rubin LH, Martin E, Weber KM, Cohen MH, Golub ET, Valcour V, Young MA,
991 Crystal H, Anastos K, Aouizerat BE, Milam J, Maki PM (2013) HIV and recent illicit drug use
992 interact to affect verbal memory in women. J Acquir Immune Defic Syndr 63:67-76.

993 Mouton PR (2002) Principles and practices of unbiased stereology: an introduction for
994 bioscientists. Baltimore: The Johns Hopkins University Press.

995 Mouton PR (2014) Neurostereology: Unbiased Stereology of Neural Systems. New York: Wiley
996 Blackwell.

997 Nath A, Hauser KF, Wojna V, Booze RM, Maragos W, Prendergast M, Cass W, Turchan JT
998 (2002) Molecular basis for interactions of HIV and drugs of abuse. J Acquir Immune Defic
999 Syndr 31 Suppl 2:S62-69.

1000 Ochs SM, Dorostkar MM, Aramuni G, Schon C, Filser S, Poschl J, Kremer A, Van Leuven F,
1001 Ovsepian SV, Herms J (2015) Loss of neuronal GSK3β reduces dendritic spine stability and
1002 attenuates excitatory synaptic transmission via β-catenin. Mol Psychiatry 20:482-489.

1003 Pelkey KA, Chittajallu R, Craig MT, Tricoire L, Wester JC, McBain CJ (2017) Hippocampal
1004 GABAergic Inhibitory Interneurons. Physiol Rev 97:1619-1747.

1005 Piepenbrink MS, Samuel M, Zheng B, Carter B, Fucile C, Bunce C, Kiebala M, Khan AA,
1006 Thakar J, Maggirwar SB, Morse D, Rosenberg AF, Haughey NJ, Valenti W, Keefer MC,
1007 Kobie JJ (2016) Humoral dysregulation associated with increased systemic inflammation
1008 among injection heroin users. PLoS One 11:e0158641.

1009 Ramage SN, Anthony IC, Carnie FW, Busuttil A, Robertson R, Bell JE (2005)

1010 Hyperphosphorylated tau and amyloid precursor protein deposition is increased in the brains
1011 of young drug abusers. Neuropathol Appl Neurobiol 31:439-448.

1012 Raybuck JD, Hargus NJ, Thayer SA (2017) A GluN2B-Selective NMDAR antagonist reverses
1013 synapse loss and cognitive impairment produced by the HIV-1 protein Tat. J Neurosci
1014 37:7837-7847.

1015 Reisine T, Pasternak G (1996) Opioid analgesics and antagonists. In: The Pharmacological
1016 Basis of Therapeutics, 9 Edition (Hardman JG, Gilman AG, Limbird LE, eds), pp 521-557.
1017 New York: McGraw-Hill Professional.

1018 Robinson TE, Gorny G, Savage VR, Kolb B (2002) Widespread but regionally specific effects of
1019 experimenter- versus self-administered morphine on dendritic spines in the nucleus
1020 accumbens, hippocampus, and neocortex of adult rats. Synapse 46:271-279.

1021 Roy DS, Kitamura T, Okuyama T, Ogawa SK, Sun C, Obata Y, Yoshiki A, Tonegawa S (2017)
1022 Distinct neural circuits for the formation and retrieval of episodic memories. Cell
1023 170:10001012 e1019.

1024 Saylor D, Dickens AM, Sacktor N, Haughey N, Slusher B, Pletnikov M, Mankowski JL, Brown A,
1025 Volsky DJ, McArthur JC (2016) HIV-associated neurocognitive disorder--pathogenesis and
1026 prospects for treatment. Nature reviews Neurology 12:234-248.

1027 Schier CJ, Marks WD, Paris JJ, Barbour AJ, McLane VD, Maragos WF, McQuiston AR, Knapp
1028 PE, Hauser KF (2017) Selective vulnerability of striatal D2 versus D1 dopamine receptor-
1029 expressing medium spiny neurons in HIV-1 Tat transgenic male mice. J Neurosci. 37:5758-
1030 5769.

1031 Sharifi KA, Rezayof A, Alijanpour S, Zarrindast MR (2020) GABA-cannabinoid interplays in the
1032 dorsal hippocampus and basolateral amygdala mediate morphine-induced amnesia. Brain
1033 Res Bull 157:61-68.

1034 Siggins GR, Zieglgänsberger W (1981) Morphine and opioid peptides reduce inhibitory synaptic
1035 potentials in hippocampal pyramidal cells in vitro without alteration of membrane potential.
1036 Proc Natl Acad Sci U S A 78:5235-5239.

1037 Smail RC, Brew BJ (2018) HIV-associated neurocognitive disorder. Handb Clin Neurol 152:75-
1038 97.

1039 Stankeviciute NM, Scofield MD, Kalivas PW, Gipson CD (2014) Rapid, transient potentiation of
1040 dendritic spines in context-induced relapse to cocaine seeking. Addict Biol 19:972-974.

1041 Vasko MR, Domino EF (1978) Tolerance development to the biphasic effects of morphine on
1042 locomotor activity and brain acetylcholine in the rat. J Pharmacol Exp Ther 207:848-858.

1043 Wersinger SR, Ginns EI, O'Carroll AM, Lolait SJ, Young WS, 3rd (2002) Vasopressin V1b
1044 receptor knockout reduces aggressive behavior in male mice. Mol Psychiatry 7:975-984.

1045 West MJ, Slomianka L, Gundersen HJ (1991) Unbiased stereological estimation of the total
1046 number of neurons in the subdivisions of the rat hippocampus using the optical fractionator.
1047 Anat Rec 231:482-497.

1048 Xu Q, Li WY, Guan Y (2013) Mu-opioidergic modulation differs in deep and superficial wide
1049 dynamic range dorsal horn neurons in mice. Neurosci Lett 549:157-162.

1050 Yuferov V, Ho A, Morgello S, Yang Y, Ott J, Kreek MJ (2013) Expression of ephrin receptors
1051 and ligands in postmortem brains of HIV-infected subjects with and without cognitive
1052 impairment. J Neuroimmune Pharmacol 8:333-344.

1053 Zhang Y, Li Q, Wen X, Cai W, Li G, Tian J, Zhang YE, Liu J, Yuan K, Zhao J, Wang W, Zhou Z,
1054 Ding M, Gold MS, Liu Y, Wang GJ (2017) Granger causality reveals a dominant role of
1055 memory circuit in chronic opioid dependence. Addict Biol 22:1068-1080.

1056 Zheng H, Zeng Y, Chu J, Kam AY, Loh HH, Law PY (2010) Modulations of NeuroD activity
1057 contribute to the differential effects of morphine and fentanyl on dendritic spine stability. J
1058 Neurosci 30:8102-8110.

1059 Zhu F, Yan CX, Zhao Y, Zhao Y, Li PP, Li SB (2011) Effects of pre-training morphine on spatial
1060 memory acquisition and retrieval in mice. Physiol Behav 104:754-760.

1061

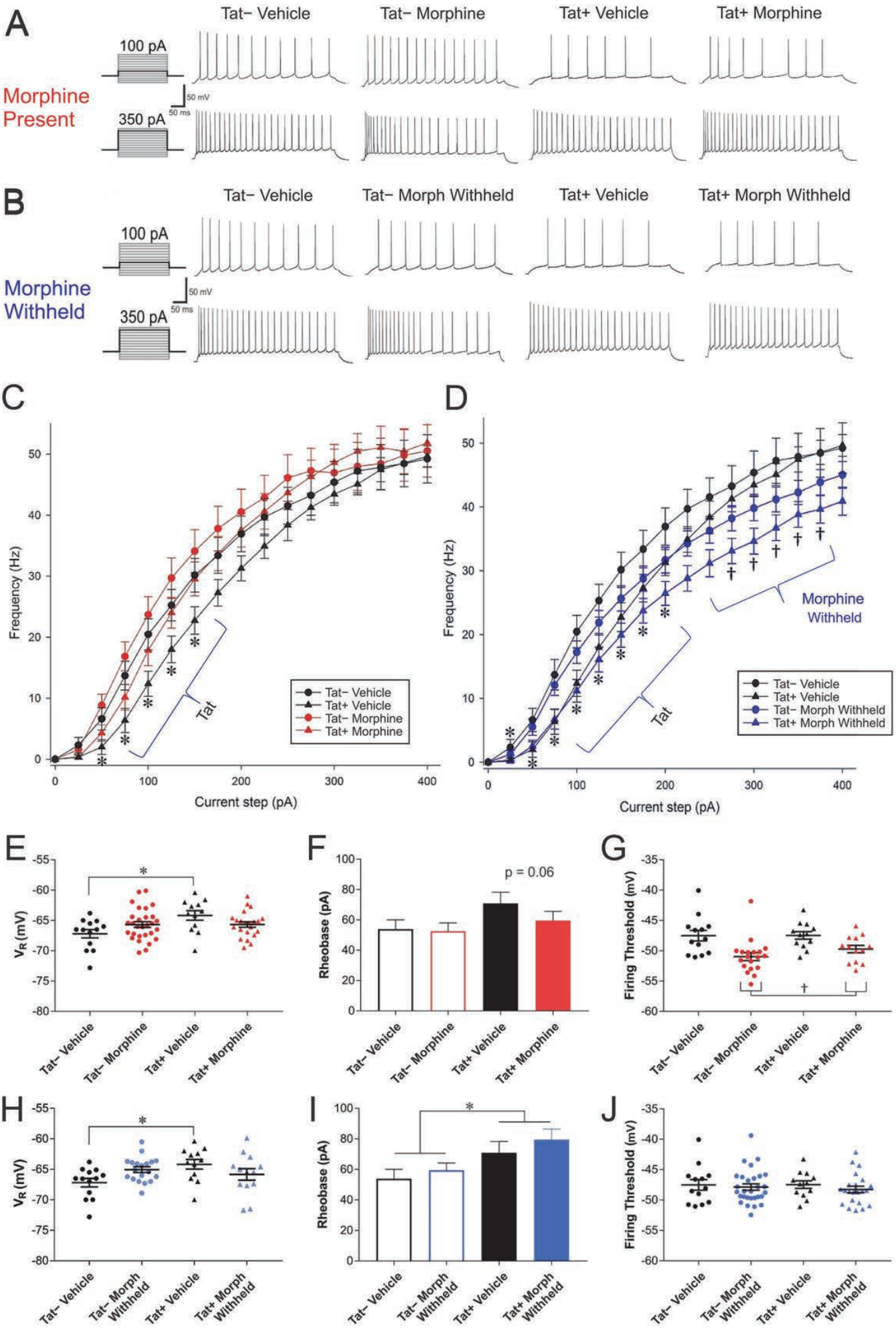

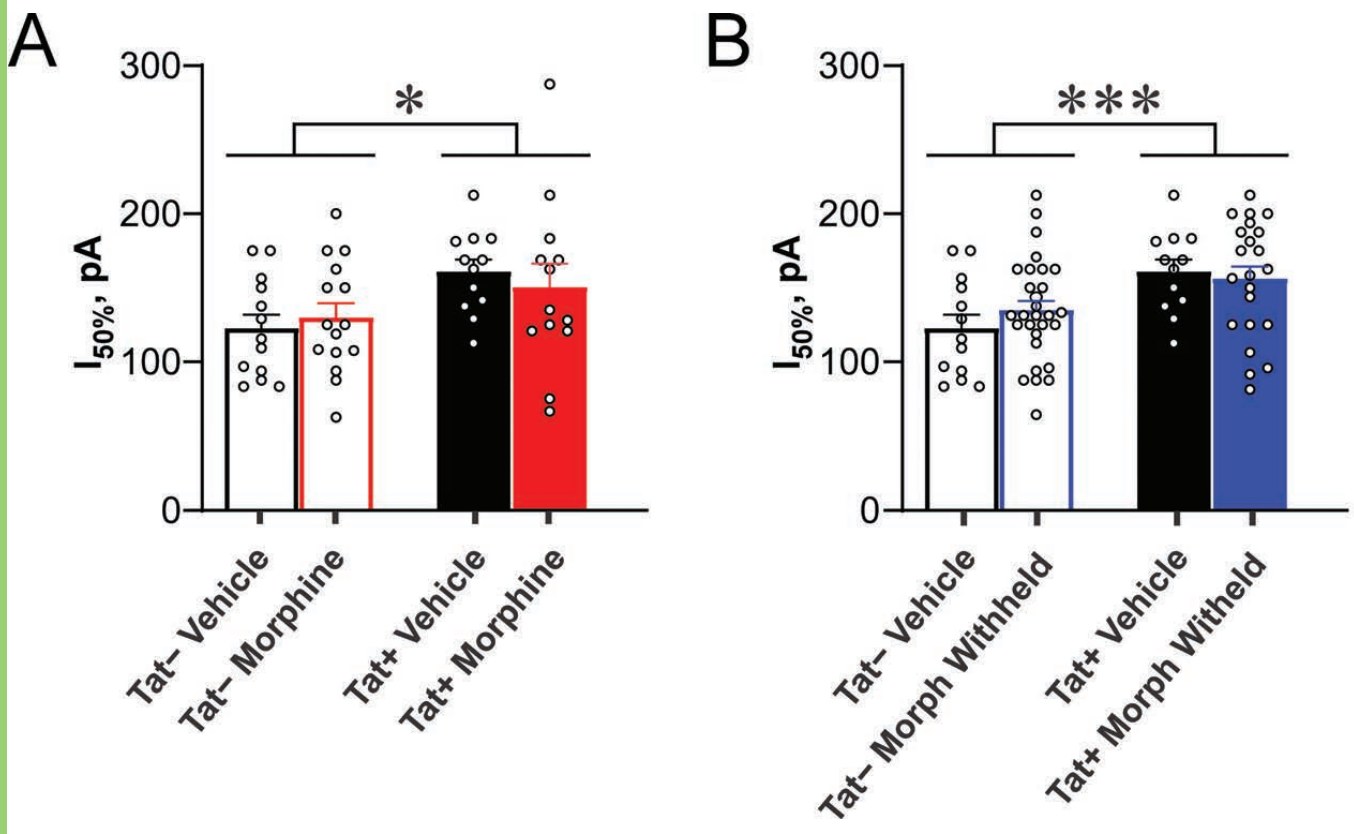

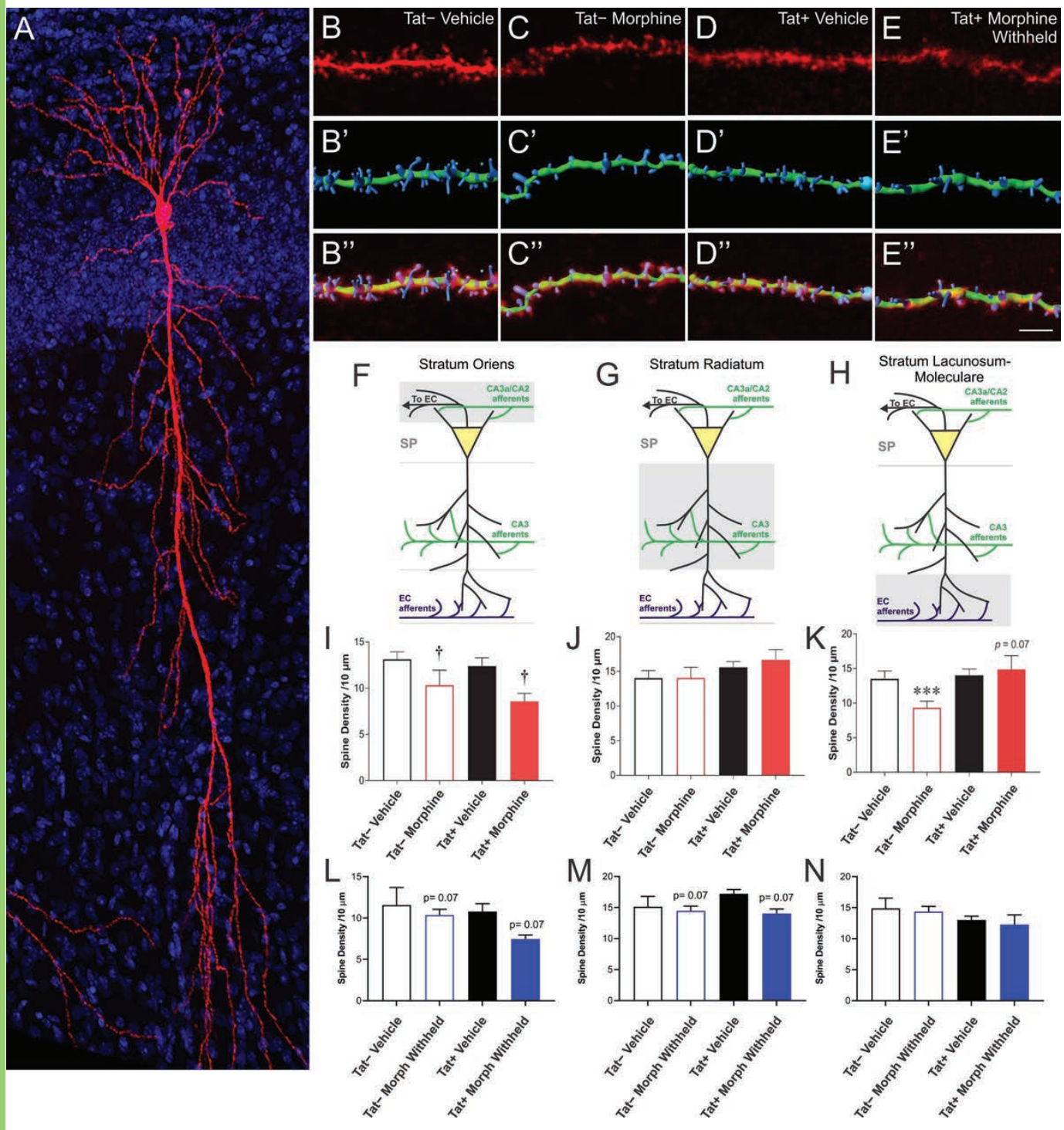

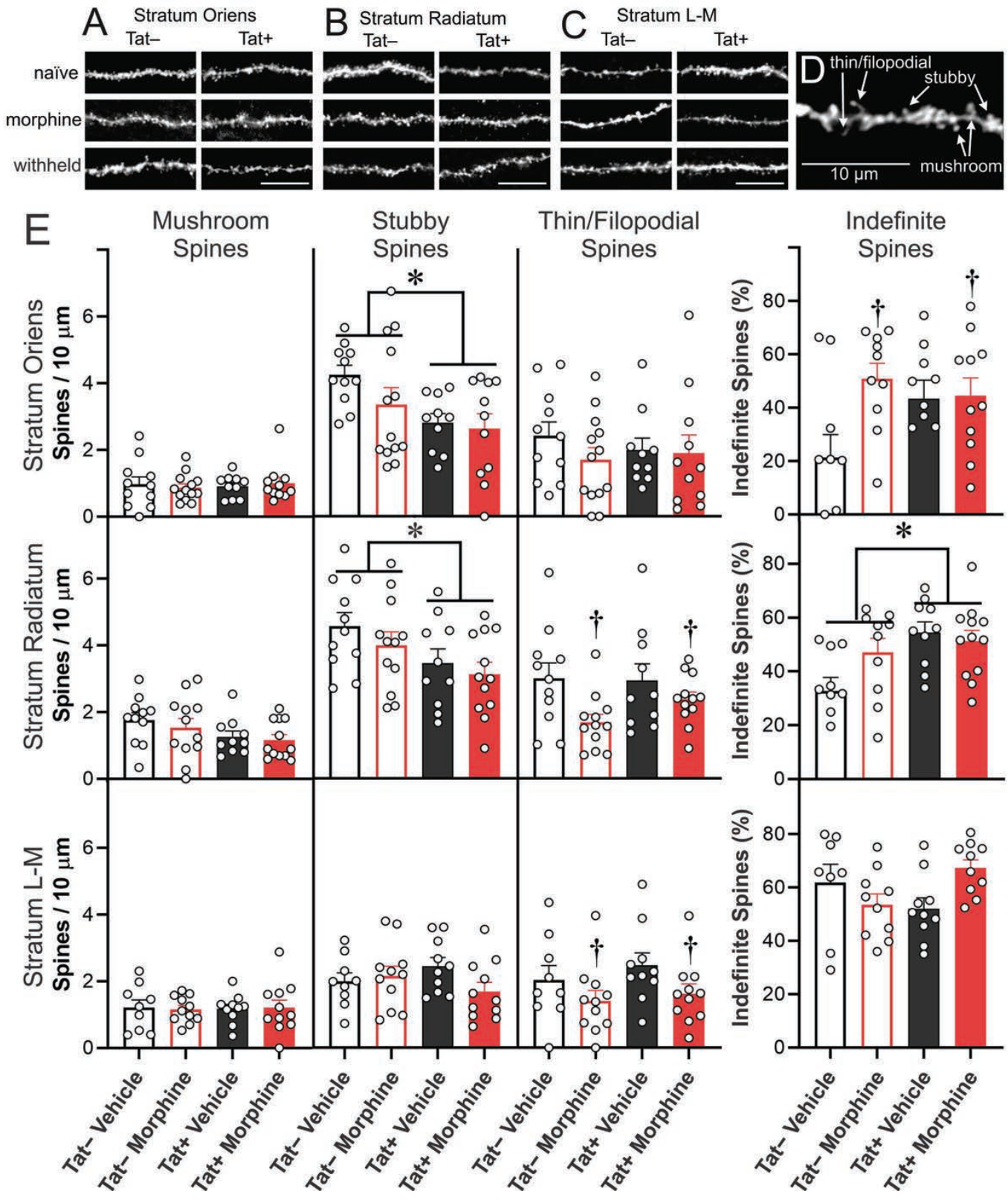

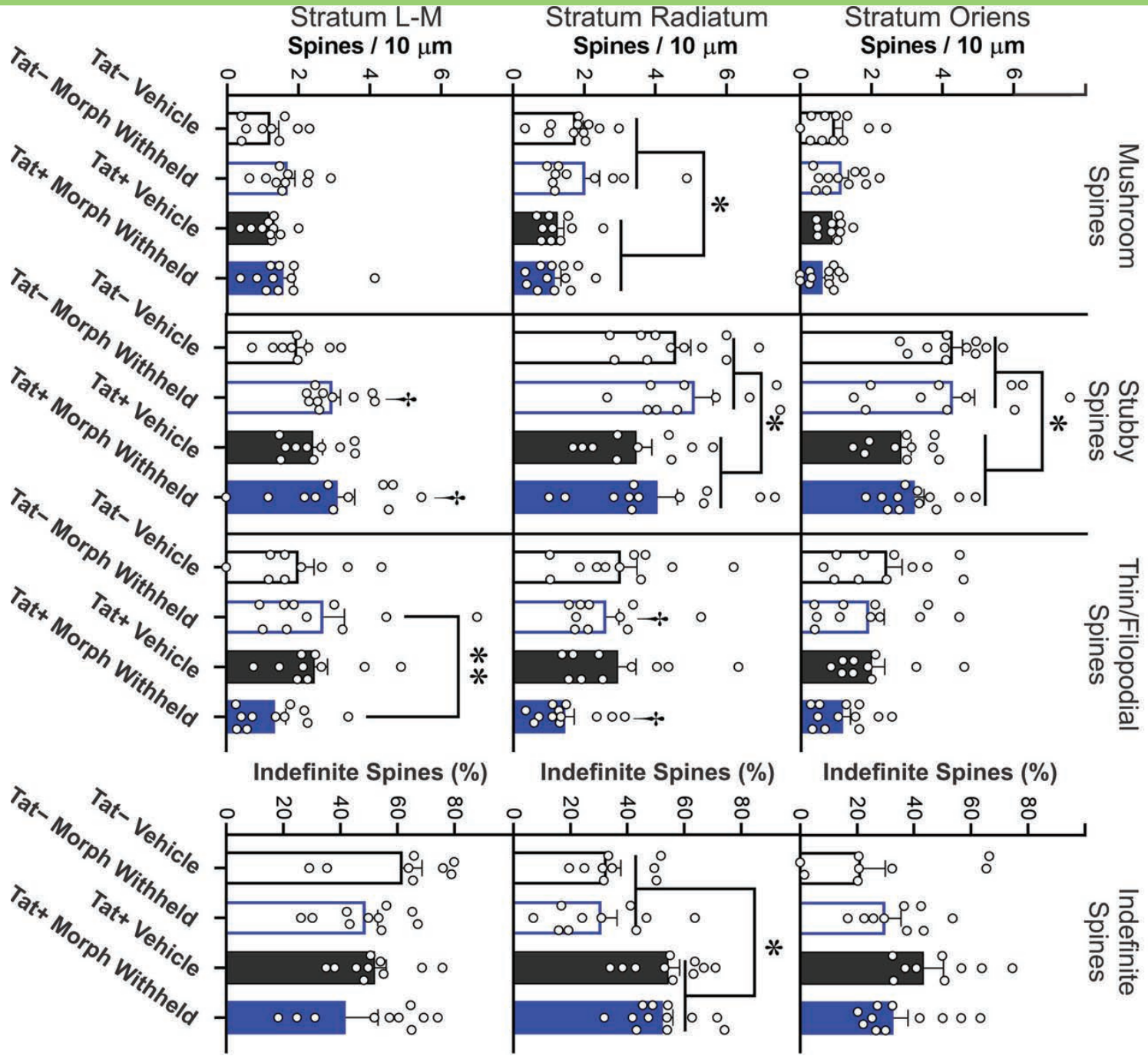

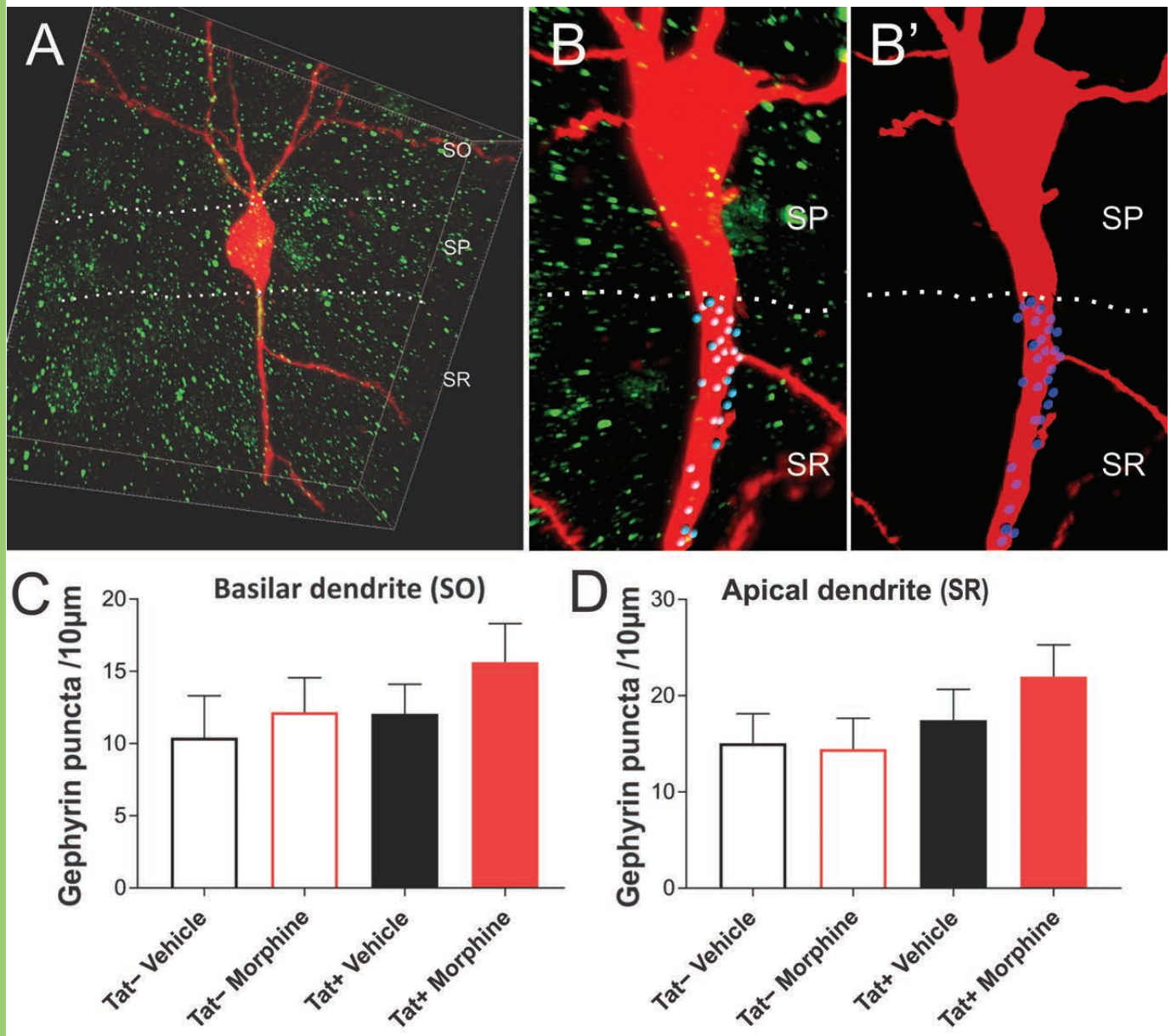

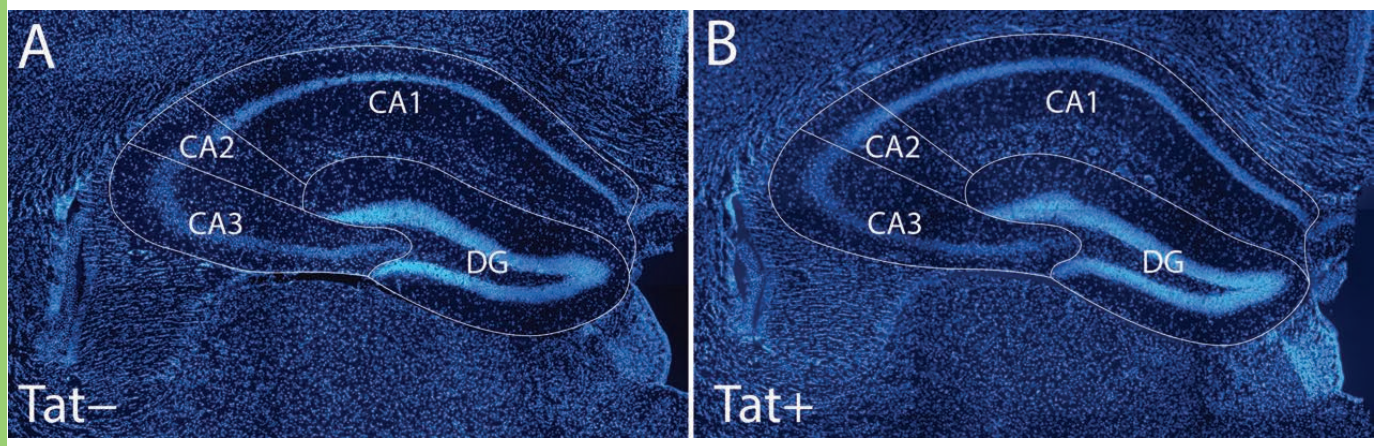

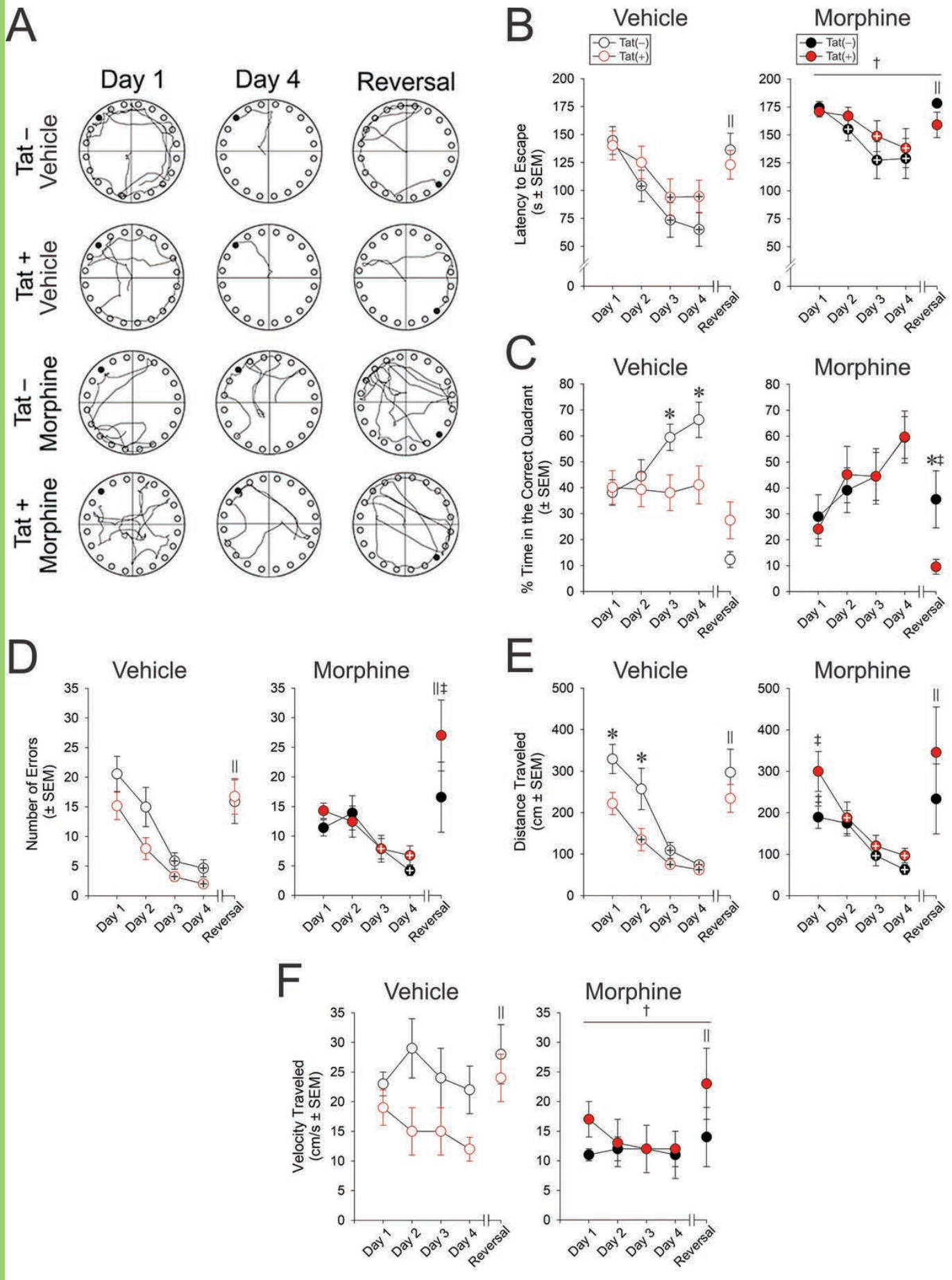

Table 1. Membrane properties of CA1 pyramidal cells after exposure to Tat and morphine

***In vivo* treatment**	**Tat− Vehicle *n* = 13**	**Tat+ Vehicle *n* = 12**	**Tat− Morphine *n* = 19**	**Tat+ Morphine *n* = 13**	**Tat− Morphine *n* = 29**	**Tat+ Morphine *n* = 22**
***Ex vivo* treatment**	**—**	**—**	morphine	morphine	**—**	**—**
Capacitance (pF)	130.2 ± 12.4	175.4 ± 16.0	157.7 ± 9.5	138.4 ± 10.3	166.3 ± 8.8	184.7 ± 13.5
Resistance (MΩ)	182.1 ± 21.6	154.7 ± 16.9	146.4 ± 10.2	127.2 ± 8.9	179.0 ± 10.9	149.2 ± 16.2

Capacitance and resistance values from pyramidal cell recordings from Tat− and Tat+ mice maintained on vehicle- (control) or morphine- (25 mg) containing time-release implants in which morphine (500 nM) was present ('morphine') or withheld (**—**) during recordings in hippocampal slices *ex vivo*. No significant changes were observed. All values are shown as mean ± SEM.

Table 2. Stereological analyses of hippocampal volume

	Tat−		Tat+	
	Vehicle	Morphine (25 mg)	Vehicle	Morphine (25 mg)
CA1	44.35 ± 2.48 %	43.97 ± 0.72 %	40.19 ± 3.48 %	46.13 ± 3.18 %
CA2	5.00 ± 0.71 %	5.03 ± 0.68 %	4.70 ± 0.65 %	5.21 ± 1.07 %
CA3	26.71 ± 1.93 %	26.58 ± 1.53 %	**35.92 ± 2.26 % ***	**28.91 ± 2.88 % ***
DG	26.94 ± 1.45 %	24.42 ± 1.24 %	28.31 ± 2.19 %	28.07 ± 2.87 %

No significant alterations in total hippocampal volume for CA1 were found in male Tat transgenic mice (n = 5-8) following 2 weeks of doxycycline and 5 d subcutaneous vehicle- or morphine- (25 mg) containing time-release implant. A significant increase in hippocampal area CA3 volume was detected for Tat+ mice. * indicates a significant difference between Tat− and Tat+ tissues, $p < 0.05$.